Basic Research in Cardiology (2022) 117:43
https://doi.org/10.1007/s00395-022-00950-7

ORIGINAL CONTRIBUTION

Acid sphingomyelinase deactivation post-ischemia promotes brain angiogenesis and remodeling by small extracellular vesicles

Ayan Mohamud Yusuf[1,2] · Nina Hagemann[1,2] · Xiaoni Zhang[1,2] · Maria Zafar[1,2] · Tanja Hussner[1,2] · Carolin Bromkamp[1,2] · Carlotta Martiny[1,2] · Tobias Tertel[3] · Verena Börger[3] · Fabian Schumacher[4,5,6] · Fiorella A. Solari[7] · Mike Hasenberg[8] · Christoph Kleinschnitz[1,2] · Thorsten R. Doeppner[1,2,9] · Burkhard Kleuser[5] · Albert Sickmann[7,10,11] · Matthias Gunzer[7,8] · Bernd Giebel[3] · Richard Kolesnick[12] · Erich Gulbins[4] · Dirk M. Hermann[1,2]

Received: 19 July 2021 / Revised: 17 July 2022 / Accepted: 8 August 2022 / Published online: 29 August 2022

Abstract

Antidepressants have been reported to enhance stroke recovery independent of the presence of depressive symptoms. They have recently been proposed to exert their mood-stabilizing actions by inhibition of acid sphingomyelinase (ASM), which catalyzes the hydrolysis of sphingomyelin to ceramide. Their restorative action post-ischemia/reperfusion (I/R) still had to be defined. Mice subjected to middle cerebral artery occlusion or cerebral microvascular endothelial cells exposed to oxygen–glucose deprivation were treated with vehicle or with the chemically and pharmacologically distinct antidepressants amitriptyline, fluoxetine or desipramine. Brain ASM activity significantly increased post-I/R, in line with elevated ceramide levels in microvessels. ASM inhibition by amitriptyline reduced ceramide levels, and increased microvascular length and branching point density in wildtype, but not *sphingomyelinase phosphodiesterase-1* ([*Smpd1*]$^{-/-}$) (i.e., ASM-deficient) mice, as assessed by 3D light sheet microscopy. In cell culture, amitriptyline, fluoxetine, and desipramine increased endothelial tube formation, migration, VEGFR2 abundance and VEGF release. This effect was abolished by *Smpd1* knockdown. Mechanistically, the promotion of angiogenesis by ASM inhibitors was mediated by small extracellular vesicles (sEVs) released from endothelial cells, which exhibited enhanced uptake in target cells. Proteomic analysis of sEVs revealed that ASM deactivation differentially regulated proteins implicated in protein export, focal adhesion, and extracellular matrix interaction. In vivo, the increased angiogenesis was accompanied by a profound brain remodeling response with increased blood–brain barrier integrity, reduced leukocyte infiltrates and increased neuronal survival. Antidepressive drugs potently boost angiogenesis in an ASM-dependent way. The release of sEVs by ASM inhibitors disclosed an elegant target, via which brain remodeling post-I/R can be amplified.

Keywords Antidepressants · Ceramide · Exosome · Focal cerebral ischemia · Sphingomyelin · Stroke recovery

✉ Dirk M. Hermann
dirk.hermann@uk-essen.de

1 Department of Neurology, University Hospital Essen, Hufelandstr. 55, 45122 Essen, Germany

2 Center for Translational and Behavioral Neurosciences, University Hospital Essen, Essen, Germany

3 Institute of Transfusion Medicine, University Hospital Essen, Essen, Germany

4 Institute of Molecular Biology, University Hospital Essen, Essen, Germany

5 Department of Toxicology, University of Potsdam, Nuthetal, Germany

6 Institute of Pharmacy, Freie Universität Berlin, Berlin, Germany

7 Leibniz-Institut für Analytische Wissenschaften-ISAS-e.V., Dortmund, Germany

8 Institute of Immunology and Experimental Imaging, University Hospital Essen, Essen, Germany

9 Department of Neurology, University Medicine Göttingen, Göttingen, Germany

10 Medizinisches Proteom-Center (MPC), Ruhr University, Bochum, Germany

11 Department of Chemistry, College of Physical Sciences, University of Aberdeen, Aberdeen, Scotland, UK

12 Memorial Sloan Kettering Cancer Center, New York, NY, USA

Introduction

Ischemic stroke is the leading cause of long-term disability and a major cause of death in humans [2]. Treatment options are limited to the acute stroke phase, in which reopening of the occluded artery by thrombolysis [18] and/or mechanical thrombectomy [38] have been shown to promote clinical recovery. Owing to reperfusion therapies, the outcome of ischemic stroke patients has considerably improved. Yet, the majority of stroke patients still exhibit neurological deficits in the long run [30, 63]. Strong efforts are currently made to establish restorative therapies that promote brain tissue remodeling and enhance neurological recovery in the post-acute stroke phase [5, 50, 59]. A safe treatment that enhances post-ischemic tissue remodeling and brain recovery would meet a major need in patient care.

Antidepressants are widely prescribed in stroke patients for the treatment of stroke-associated depression [2]. Two antidepressants, the serotonin reuptake inhibitor fluoxetine and the monoamine reuptake inhibitor nortriptyline, which is the active metabolite of amitriptyline, enhanced clinical stroke recovery independent of the presence of depressive symptoms in some [7, 24, 41, 45], but not other [11, 13] randomized placebo-controlled studies. Antidepressants are believed to act via the modulation of monoaminergic neurotransmitter systems [26]. Experimental studies more recently proposed an essential role of acid sphingomyelinase (abbreviated ASM for the human protein, abbreviated Asm for the murine protein) in mediating antidepressant drug effects [26]. ASM hydrolytically cleaves sphingomyelin to ceramide, which is a constituent of membrane microdomains that profoundly control cell signaling processes [9, 57]. In a model of unpredictable stress-induced depression, the antidepressants amitriptyline and fluoxetine, which are diverse in their neurotransmitter mode of action, inhibited cerebral Asm activity, restored neuronal proliferation and differentiation in the hippocampus and reversed depressive-like behaviors [17]. In mice lacking Asm, both antidepressants did not increase neuronal proliferation and differentiation and did not reverse depressive-like behaviors [17].

Following focal and global cerebral ischemia, Asm activity and ceramide level have been shown to be increased in the ischemic mouse and rat brain [3, 19, 39, 61]. After transient middle cerebral artery occlusion (MCAO), genetic Asm deficiency reduced infarct volume, neurological deficits and proinflammatory cytokine abundance in the acute stroke phase, that is, 24 h post-stroke [61]. The role of the Asm/ceramide system in brain tissue remodeling in the post-acute stroke phase had so far not been studied. In the present study, we examined effects of Asm inhibitors, many of which are clinically used as antidepressants, on cerebral angiogenesis, brain tissue remodeling and functional recovery after focal cerebral ischemia/reperfusion (I/R). Following observations that chemically and pharmacologically diverse antidepressants amplified cerebral angiogenesis when administered in the stroke recovery phase, we discovered a novel mechanism via which ASM/ceramide inhibition induces the formation and release of small extracellular vesicles (sEVs) by human cerebral microvascular endothelial cells, which have *bona fide* characteristics of exosomes and which, as we further show, promote angiogenesis. Angiogenesis plays a central role in the remodeling of brain tissue post-I/R. Thus, newly formed microvessels (1) release growth factors that prevent delayed brain atrophy and promote neuronal plasticity, (2) act as scaffolds for the migration of neural progenitor cells which promote neuronal plasticity, and (3) contribute to removal of necrotic brain tissue by enabling macrophage infiltration [25, 33, 47, 51].

Materials and methods

Legal issues, animal husbandry and randomization

Experiments were performed with local government approval (State Agency for Nature, Environment and Consumer Protection, Recklinghausen) in accordance to E.U. guidelines (Directive 2010/63/EU) for the care and use of laboratory animals. Experiments were strictly randomized and blinded at all stages of the study. In the animal experiments, the investigator performing the surgeries and histochemical studies (A.M.Y.) was blinded by another researcher (N.H.) preparing the treatment solutions, which received dummy names (solution A, B, C) and were decoded after termination of the study. Animals were kept in a regular 12 h:12 h light/dark cycle in groups of 5 animals/cage with free access to food and water. Throughout the study, the animals had free access to food and water. The data that support the findings of this study are available from the corresponding author upon reasonable request.

Middle cerebral artery occlusion (MCAO)

Focal cerebral ischemia was induced in male C57BL/6j wildtype mice (8–10 weeks; 22–25 g; Harlan Laboratories, Darmstadt, Germany), in *sphingomyelinase phosphodiesterase-1* [*Smpd1*]$^{-/-}$) (that is, ASM deficient) mice on C57BL/6j background and their *Smpd1*$^{+/+}$ C57BL/6j littermates by 20 min left-sided intraluminal MCAO or 40 min left-sided intraluminal MCAO for the assessment of neurological recovery [44, 58]. Mice were anesthetized with 1.0–1.5% isoflurane (30% O_2, remainder N_2O). Rectal

temperature was maintained between 36.5 and 37.0 °C using a feedback-controlled heating system. Cerebral blood flow was recorded by laser Doppler flow (LDF) measurement using a flexible probe with a diameter of 0.5 mm attached to the animals' skull above the core of the middle cerebral artery territory. For MCAO, a midline neck incision was made and the left common and external carotid arteries were isolated and ligated. The internal carotid artery (ICA) was temporally clipped. A silicon-coated monofilament was introduced via a small incision into the common carotid artery (CCA) and advanced to the carotid bifurcation for MCAO. Reperfusion was initiated by monofilament removal. Starting immediately after reperfusion onset (animal sacrifice after 24 h) or 24 h after reperfusion (animal sacrifice after 14 or 28 days), vehicle, amitriptyline (2 or 12 mg/kg b.w.; Sigma-Aldrich, Deisenhofen, Germany) or fluoxetine (10 mg/kg b.w. Sigma-Aldrich) were intraperitoneally administered for up to 28 days. Wounds were carefully sutured. The opioid buprenorphine (0.1 mg/kg; Reckitt Benckiser, Slough, U.K.) was subcutaneously administered before surgery, and the antiphlogistic carprofen (4 mg/kg; Bayer Vital, Leverkusen, Germany) was subcutaneously administered daily for up to 3 days after surgery. At the indicated timepoints, animals were deeply anesthetized with isoflurane and transcardially perfused with 40 ml 0.1 M phosphate-buffered saline (PBS) (animals used for histochemistry, activity assays and mass spectrometry) or with 40 ml 0.1 M PBS supplemented with heparin (50 U/ml) followed by 40 ml 4% paraformaldehyde (PFA) in 0.1 M PBS (animals used for light sheet microscopy).

Infarct volumetry

Brains perfused with 0.1 M PBS were frozen on dry ice and cut into 20 µm thick coronal sections. Sections were collected at 1 mm intervals for cresyl violet staining. On these sections, the border between infarcted and non-infarcted tissue was outlined using Image J (National Institutes of Health [NIH], Bethesda, MD, U.S.A.). Infarct volume was determined by subtracting the volume of the non-lesioned ipsilateral hemisphere from the volume of the contralateral hemisphere [58]. Edema volume was calculated as volume difference between the ipsilateral and the contralateral hemisphere [58].

Neurological score

General and focal neurological deficits were evaluated according to the Clark's score at baseline (i.e., 1 day before MCAO), on day 1, day 3, day 7 post-I/R and at weekly intervals thereafter until day 28 post-I/R [8].

Tight rope test

The tight rope test consists of a 60-cm-long rope connected to a platform. Mice were placed in the middle of the rope which they grasped with both forepaws. The time until they reached the platform in the end of the rope was analyzed. The maximum testing time was 60 s [58]. After baseline assessment, mice were tested on day 1 post-I/R and weekly until day 28 post-I/R.

Rotarod test

The Rotarod consists of a rotating drum (Ugo Basile, model 47,600, Comerio, Italy). Its speed increases linearly from 4 to 30 rpm. The time until the animals dropped off the drum was measured. The maximum testing time was 300 s [58]. After baseline assessment, mice were tested on day 1 and weekly until day 28 post-I/R.

FITC–albumin hydrogel perfusion and whole-brain clearing

Immediately following transcardiac PFA fixation, 10 ml of a hand-warm (30 °C) 2% gelatin hydrogel containing 0.1% FITC-conjugated albumin, which had been filtered using Whatman filter paper (GE Healthcare Life Science, Little Charfont, U.K.) and was protected from light, was transcardially infused into the animals' aorta. Brains were subsequently removed, post-fixed overnight at 4 °C in 4% PFA in 0.1 M PBS and dehydrated through a 30%, 60%, 80% and 100% tetrahydrofuran (THF; Sigma-Aldrich) gradient [32]. Brain clearing was achieved with ethyl cinnamate (ECI; Sigma-Aldrich).

3D light sheet fluorescence microscopy (LSM) and microvasculature analysis

The FITC–albumin labeled vasculature of cleared brains was scanned by a light sheet microscope (Ultramicroscope II, LaVision BioTec, Göttingen, Germany) that was equipped with a 488 nm laser. Horizontal overview images of the cleared brain were taken using a 1.6 × objective. Serial images of the striatum and cortex were acquired at 2 µm steps using a 6.4 × objective. In each animal, two regions of interest (ROI) measuring 500 µm × 500 µm × 1000 µm (in the X, Y and Z planes, respectively) in the dorsolateral striatum were analyzed using Imaris (Bitplane, Zurich, Switzerland) software with 3D rendering software package, as described previously [32]. Following image segmentation, skeletonization and 3D reconstruction, microvascular network characteristics, that is, microvascular length, branching point number and mean branch length between two branching points, were determined.

Cell culture

Immortalized brain microvascular endothelial cells (hCMEC/D3) were cultured in endothelial basal medium (EBM-2, Lonza, Basel, Schweiz) supplemented with 5% fetal bovine serum (FBS, Life Technologies, Carlsbad, CA, U.S.A.), 100 U/ml penicillin/streptomycin (Life Technologies), 1.4 µM hydrocortisone (Sigma-Aldrich), 5 µg/ml ascorbic acid (Sigma-Aldrich), 1% chemically defined lipid concentrate (Life Technologies), 10 mM HEPES (Life Technologies) and 1 ng/ml basic fibroblast growth factor (bFGF, Sigma-Aldrich). hCMEC/D3 were seeded on 150 µg/ml collagen (R&D Systems, Minneapolis, MN, U.S.A.) precoated flasks and kept at 37 °C at 5% CO_2. Oxygen–glucose deprivation (OGD) was induced by incubating the cells in a hypoxia chamber (1% O_2, Toepffer Lab Systems, Göppingen, Germany) with glucose-free medium (Life Technologies). For comparative studies on sphingomyelinase expression and activities, primary human brain microvascular endothelial cells (HBMEC; catalog #1000; ScienCell™ Research Laboratories, Carlsbad, CA, U.S.A.) cultured in endothelial cell growth medium MV (ECGM-MV, PromoCell, Heidelberg, Germany) containing 100 U/ml penicillin/streptomycin (Life Technologies) and growth medium MV supplement mix (PromoCell) and human umbilical vein endothelial cells (HUVEC) cultured in endothelial cell growth medium (ECGM, PromoCell) containing 100 U/ml penicillin/streptomycin (Life Technologies) and growth medium supplement mix (PromoCell) were used.

Small interfering RNA (siRNA) knockdown

ASM knockdown in vitro was achieved by small interfering RNA (siRNA). Transfections were performed according to the manufacturer's instructions using Dharmafect transfection reagents (Dharmacon, Lafayette, CO, U.S.A.). Scrambled siRNA was used as a negative control.

Tube formation assay

To evaluate the formation of capillary-like tubular structures [22], 60 µl matrigel (Corning, NY, U.S.A.) were pipetted into 96-well plates. The gel solidified at 37 °C for 30 min. 3×10^4 cells were seeded and treated with ASM inhibitors and/or sEVs of interest. After 20 h, photomicrographs were taken with a 2× objective using the EVOS digital inverted microscope (Advanced Microscopy Group, Bothell, WA, U.S.A.). Closed tubes were counted using Image J (NIH) in each well. Microvascular length and branching point density were evaluated. Experiments were done in triplicates for which mean values were formed.

Transwell migration assay

Cell migration was assessed using a modified Boyden chamber. 3×10^4 cells were seeded in the upper compartment of polycarbonate membrane inserts (8.0 µm pores) that contained serum-reduced (1.25% FBS) medium. Treatments of interest were administered into the lower compartment that contained 5% FBS. Cells that did not migrate were removed after 24 h. Migrated cells were fixed with 4% PFA and stained with Hoechst 33342 (Thermo Fisher Scientific, Waltham, MA, U.S.A.). Photomicrographs were taken with a 20× objective using the EVOS digital inverted microscope (Advanced Microscopy Group). In each chamber, migrated cells were counted using Image J (NIH) in 8 ROIs measuring 530 × 400 µm. Experiments were done in duplicates for which mean values were formed.

Cell viability assay

2×10^4 hCMEC/D3 were seeded into 96-well plates and treated with ASM inhibitors and/or sEVs of interest. After 24 h, cells were incubated with 0.5 mg/ml 3-(4,5-dimethyl-2-thiazolyl)-2,5-diphenyl-2H-tetrazolium bromide (MTT; Biomol, Hamburg, Germany) for 2 h. Formazon formation was measured at 570 nm on a microplate reader (iMark Detection; Bio-Rad Laboratories, Hercules, CA, U.S.A.). Samples were analyzed in triplicates, of which mean values were formed.

Sphingomyelinase activity assays

Brain samples obtained from the ischemic or contralateral middle cerebral artery territory or hCMEC/D3, HBMEC and HUVEC were lysed in 250 mM sodium acetate buffer (pH 5.0) containing 1% NP-40 detergent (Fluka BioChemika, Morristown, NJ, U.S.A.; for ASM activity measurement) or in 100 mM HEPES buffer (Life Technologies) (pH 7.4) containing 5 mM magnesium chloride (Sigma-Aldrich) and 0.1% NP-40 detergent (Fluka BioChemika; for neutral sphingomyelinase [NSM] activity measurement). The cellular membrane integrity was disrupted with a sonicator. After centrifugation for 5 min at 300*g* at 4 °C, supernatants were collected. Lysates were adjusted to a specific protein concentration and incubated with 100 pmol BODIPY-labeled sphingomyelin (Thermo Fisher Scientific) in 250 mM sodium acetate (pH 5.0) and 0.1% NP-40 for 1 h at 37 °C. Chloroform:methanol (2:1, v/v) was added, samples were vortexed and centrifuged for 5 min at 15,000 g to achieve a phase separation. The lower phase was collected and concentrated in a vacuum centrifuge (SPC111V, Thermo Fisher Scientific) for 45 min at 37 °C. Lipids were dissolved in 20 µl chloroform:methanol (2:1, v/v) and spotted onto thin layer chromatography (TLC) plates (Macherey

Nagel, Düren, Germany). The TLC run was performed with chloroform:methanol (80:20, v/v). TLC plates were analyzed with a Typhoon FLA 9500 scanner (GE Healthcare Life Sciences) and lipid spots were quantified with Image Quant (GE Healthcare Life Sciences).

Real-time quantitative polymerase chain reaction

RNA was isolated according to the phase extraction method using Trizol (Life Technologies)/Chloroform (Sigma-Aldrich) and treated with DNase I (Life Technologies). Complementary DNA (cDNA) was generated by reverse transcription with SuperScript II (Life Technologies) using oligo(dt) primers and random hexamers. Real-time quantitative polymerase chain reaction (RT-qPCR) was performed with SYBR-Green (Life Technologies) in a StepOnePlus real-time PCR system with primers for human *SMPD1* (Gene bank number: NM_000543, Biomol), human *SMPD2* (Gene bank number: NM_003080, Biomol), human *SMPD3* (Gene bank number: NM_018667, Biomol) and human *β-actin* (Gene bank number: NM_001101.2, Biomol) as a housekeeping gene. Results were quantified using the $2^{-\Delta\Delta Ct}$ method. Samples were analyzed in triplicates, of which mean values were formed.

Liquid chromatography tandem–mass spectrometry (LC–MS/MS) of sphingolipids

Following lipid extraction with methanol:chloroform (2:1, v/v) as described [16], ceramides and sphingomyelins were quantified by LC–MS/MS using a 6490 triple–quadrupole mass spectrometer (Agilent Technologies, Waldbronn, Germany) operating in the positive electrospray ionization mode (ESI +) [36]. Quantification was performed with MassHunter Software (Agilent Technologies). Sphingolipid amounts were normalized to protein content (in vivo experiments) or cell numbers (in vitro experiments. As such, concentrations per mg protein (in vivo experiments) or per 1 million cells (in vitro experiments) were calculated.

Immunohistochemistry/ immunocytochemistry

Coronal brain sections obtained from the level of the mid-striatum (bregma 0.0 mm; that is, the core of the middle cerebral artery territory) or hCMEC/D3 seeded on sterile coverslips were fixed with 4% PFA in 0.1 M PBS and immersed in 0.1 M PBS containing 0.1% Triton X-100, 5% normal donkey serum or 10% normal goat serum and 1 or 2.5% bovine serum albumin. Samples were incubated overnight at 4 °C in mouse anti-NeuN (A60; Merck Millipore, Burlington, MA, U.S.A.), rat anti-CD31 (MEC 13.3; BD Biosciences, Franklin Lakes, NJ, U.S.A.), rat anti-CD45 (30-F11; BD Biosciences, Franklin Lakes, NJ, U.S.A.), biotinylated goat anti-IgG (sc-2039; Santa Cruz, Heidelberg, Germany), mouse anti-ceramide (S58-9; Glycobiotech, Kükels, Germany), rabbit anti-apoptosis-inducing factor (AIF; D39D2; Cell Signaling Technology, Danvers, MA, U.S.A.), rabbit anti-early endosome antigen-1 (EEA1; C45B10; Cell Signaling Technology), rabbit anti-lysosomal-associated membrane protein-1 (LAMP1; 1D4B; Abcam, Cambridge, U.K.), rabbit anti-microtubule-associated protein light chain-3b (LC3b; 2775; Cell Signaling Technology), rabbit anti-caveolin (3238S; Cell Signaling Technology), rabbit anti-Rab7 (D95F2; Cell Signaling Technology) or rabbit anti-CD63 (LS-C204227; Lifespan Biosciences, Seattle, WA, U.S.A.) antibody. Samples were rinsed and labeled with appropriate secondary Alexa Fluor-594, Alexa Fluor-488, Cy3 or biotinylated antibody. In sections stained with fluorescent antibody, nuclei were counterstained with Hoechst 33342 (Thermo Fisher Scientific). Sections stained with biotinylated antibody were revealed by 3,3´-diaminobenzidine (DAB) staining using a avidin–biotin complex (ABC) peroxidase kit (Vectastain Elite Kit Standard, Vector Laboratories, Burlingame, CA, U.S.A.). Sections were evaluated using an inverted microscope equipped with apotome optical sectioning (Axio Observer.Z1; Carl Zeiss, Oberkochen, Germany). Sections were analyzed by counting the density of labeled microvessels or cells (NeuN, CD45) in the ischemic and contralateral striatum (in vivo studies) or by counting intracellular vesicles (ceramide) in 8 ROIs measuring 135 × 135 µm on coverslips (in vitro studies). Cells were randomly selected and not pre-selected based on the presence of ceramide-rich vesicles. IgG immunohistochemistry was examined by densitometry in the ischemic and contralateral striatum [20].

Western blot analysis of cell lysates

Cells were lysed with NP-40 buffer containing protease and phosphatase inhibitors (Sigma-Aldrich). Lysates were centrifuged at 13,400 rpm at 4 °C and the supernatant was collected. Equal amounts of protein were separated by sodium dodecyl sulfate–polyacrylamide gel electrophoresis (SDS–PAGE) and subsequently transferred to nitrocellulose membranes (GE Healthcare Life Science). Non-specific binding was blocked with 5% non-fat milk powder (Sigma-Aldrich) dissolved in 0.1% Tween in 0.1 M Tris-buffered saline (TBS-T). Membranes were incubated with rabbit anti-vascular endothelial growth factor (VEGF) receptor-2 (VEGFR2) (55B11; Cell Signaling Technology), goat anti-ASM (AF5348, R&D Systems) and rabbit anti-β-actin (4967; Cell Signaling Technology) antibody overnight at 4 °C, rinsed and incubated in peroxidase-conjugated secondary antibodies (Santa Cruz, Heidelberg, Germany) for 1 h at room temperature. Signals were detected by enhanced chemiluminescence using prime Western blotting detection

reagent (GE Healthcare Life Science). VEGFR2 and ASM expression were normalized to β-actin abundance.

Enzyme-linked immunosorbent assay (ELISA)

VEGF was quantified by ELISA (R&D Systems) in supernatants of hCMEC/D3 in accordance to the manufacturer's instruction. Amitriptyline was determined by ELISA (Lifespan Biosciences) in cell samples of hCMEC/D3 in accordance to the manufacturer's instruction.

Preparation of small extracellular vesicles (sEVs)

hCMEC/D3 were cultured in triple flasks (Thermo Fisher Scientific). Media were collected after exposure of cells to the different experimental conditions and centrifuged at 2,000 g for 15 min at 4 °C, followed by centrifugation at 10,000*g* for 45 min at 4 °C (5810R centrifuge, Eppendorf, Hamburg, Germany). Supernatants were filtered through a 0.22 µm filter (Sartorius, Göttingen, Germany) and supplemented with NaCl at a final concentration of 75 mM and polyethylene glycol-6000 (PEG; Sigma-Aldrich) at a final concentration of 10%. sEVs were concentrated at 1,500 g for 30 min at 4 °C (Avanti J-26 XP centrifuge, Beckmann Coulter, Brea, CA, U.S.A.). Pellets were then dissolved in 0.9% NaCl (Sigma-Aldrich), transferred to ultra-clear centrifuge bottles (Beckmann Coulter) and precipitated by ultracentrifugation at 110,000*g* for 130 min at 4 °C (Optima L7-65, k factor: 133, Beckmann Coulter). sEV pellets were resuspended in 0.9% NaCl supplemented with 10 mM HEPES (Life Technologies) and stored in low retention microcentrifuge tubes (Kisker Biotech, Steinfurt, Germany) at -80 °C until further use.

Amnis ImagestreamX flow cytometry of sEVs

sEVs were quantified with an ImageStreamX MkII instrument (Merck Millipore) as described previously [14] after CD9–FITC (MEM-61; Exbio, Vestec, Czech Republic) and CD63–APC (MEM-259; Exbio) antibody staining. All samples were appropriately diluted to avoid coincidence or swarm detection. Data analysis was performed using Amnis IDEAS software (version 6.1).

sEV uptake analysis

Following sEV preparation by PEG precipitation and ultracentrifugation from the supernatant of hCMEC/D3, as described, sEV preparations were labeled with PKH67 membrane dye (Sigma-Aldrich). Briefly, sEV preparations were stained with 2 µM PKH67 diluted in diluent C for 5 min at room temperature. Excess dye was removed by washing twice with PBS using Amicon-Ultra Centrifugal Filter Units (Merck Millipore). Labeled sEVs were incubated with hCMEC/D3 for 24 h. Cells were fixed with PFA, labeled with rabbit anti-Rab7 (D95F2; Cell Signaling Technology), rabbit anti-CD63 (LS-C204227; Lifespan Biosciences) or rabbit anti-LAMP1 (1D4B; Abcam) antibody, detected by appropriate secondary antibody (as above) and counterstained with Hoechst 33342 (Thermo Fisher Scientific).

Characterization of sEV preparations by nanoparticle tracking analysis (NTA)

According to recently updated guidelines for the characterization of small extracellular vesicles [52], sEV preparations were analyzed for concentration and size by nanoparticle tracking analysis (NTA; Particle Metrix, Meerbusch, Germany), as described previously [49].

Western blot analysis of sEV preparations

Protein concentrations in sEV preparations were determined by a standardized bicinchoninic acid (BCA) assay according the manufacturer's protocol (Pierce, Rockford, IL, U.S.A.). For Western blot, 30 µg protein samples were solubilised with Laemmli sample buffer under reducing (containing dithiothreitol [DTT]; AppliChem, Darmstadt, Germany) or non-reducing (not containing DTT) conditions and separated on SDS–PAGE gels before transfer to polyvinylidene fluoride membranes (PVDF; Millipore, Darmstadt, Germany). Membranes were blocked in TBS-T supplemented with 5% (*w*/*v*) skim milk powder (Sigma-Aldrich). Membranes were stained with rabbit anti-syntenin (clone EPR8102; Abcam), rabbit anti-calnexin (ab10286; Abcam) or mouse anti-CD9 (clone VJ1/20.3.1; kindly provided by Francisco Sánchez, Madrid, Spain) antibodies. Anti-syntenin and anti-CD9 antibodies were used as sEV markers, anti-calnexin antibody as cellular contamination marker. Membranes were washed and counterstained with appropriate horseradish peroxidase-conjugated secondary antibodies (Santa Cruz) that were detected by enhanced chemiluminescence using prime Western blotting detection reagent (GE Healthcare Life Science).

Transmission electron microscopy of sEV preparations

200 mesh copper grids (Plano, Wetzlar, Germany) were physically charged by a glow discharge procedure to allow strong adherence of particles to the electron microscopy grid during further processing. 4.5 µl of sEV preparations were added to the pre-treated grid surface and dried at room temperature. For subsequent removal of salts, grids were successively transferred on three droplets of deionized water. Samples were incubated with 1.5% phosphotungstate acid

(Electron Microscopy Science, Hatfield, PA, U.S.A.) and dried. Images were acquired using a JEM 1400Plus electron microscope (JEOL, Tokyo, Japan) operating at 120 kV that was equipped with a 4096 × 4096 pixel CMOS camera (TemCam-F416; TVIPS, Gauting, Germany). Image acquisition software EMMENU (Version 4.09.83) was used for taking 16 bit images. Image post-processing was carried out using ImageJ software (Version 1.52b; NIH).

LC–MS-based proteomics

For label free proteome analysis, sEV preparations obtained from supernatants of hCMEC/D3, which were cultured under normoxic conditions and exposed to vehicle or amitriptyline (50 µM), were lysed in 50 mM Tris–HCl, 150 mM NaCl and 1% sodium dodecyl sulfate (SDS) at pH 7.8 supplemented with 1 tablet cOmplete Mini and 1 tablet PhosSTOP (Roche, Basel, Switzerland) per 10 ml. Protein concentrations were determined using the bicinchoninic acid assay (Pierce, Thermo Fisher Scientific). Afterwards, cysteines were reduced by 30 min incubation at 56 °C with 10 mM dithiothreitol and free sulfhydryl groups were alkylated with 30 mM iodoacetamide for 30 min at room temperature in the dark. Samples were processed using S-trap Micro Column Digestion Protocol (PROTIFI, Farmingdale, NY, USA) according to the manufacturer's instructions [31] with slight modifications. In brief, carbamidomethylated samples were diluted with 10% SDS to a final concentration of 5% SDS. Afterwards, 4.43 µl of 12% phosphoric acid were added, followed by the addition of 292.38 µl of S-trap binding buffer (90% methanol, 100 mM triethylammonium bicarbonate (TEAB), pH 7.1). 165 µl of the acidified lysate/S-trap buffer mix was placed into the spin column and spun down in a bench-top centrifuge in a 1.5 ml tube at 4000*g* until all the solution had passed through. The flow through was discarded and the rest of the acidified lysate/S-trap buffer mix was loaded into the spin column and the procedure explained before was repeated.

Afterwards, 3 washing steps with 150 µl of S-trap binding buffer each were performed by centrifugation at 4,000 g. Then, sequencing grade modified trypsin (Promega, Madison, WI, U.S.A.) was added in an enzyme to a sample ratio of 1:10 (w/w) in 25 µl of 50 mM ammonium bicarbonate (ABC) containing 2 mM $CaCl_2$. Spin columns were incubated for 1 h at 47 °C. After incubation, peptides were recovered by centrifugation prior addition of 40 µl of 50 mM ABC to the spin columns. Further peptide recovery was done by adding 40 µl 0.1% of trifluoroacetic acid (TFA) and 35 µl of 50% acetonitrile (for recovering hydrophobic peptides) to the spin columns followed by centrifugation. Finally, samples were dried under vacuum and resuspended in 0.1% TFA. Digestion quality control was performed via a monolithic column–HPLC [4]. NanoLC–MS/MS analysis was done using a U3000 RSLCnano online-coupled to a Q Exactive HF mass spectrometer (Thermo Fisher Scientific). Thus, peptides samples were loaded onto the trap column (Acclaim PepMap100 C18; 100 µm × 2 cm) in 0.1% TFA at a flow rate of 20 µl/min. After 5 min, the pre-column was switched in line with the main column (Acclaim PepMap100 C18; 75 µm × 50 cm) and peptides were separated using a 100 min binary gradient ranging from 5–24–40 of 84% acetonitrile in 0.1% formic acid at 60 °C and a flow rate of 250 nl/min. The MS was operated in data dependent acquisition (DDA) mode with survey scans acquired at a resolution of 60,000 followed by 15 MS/MS scans at a resolution of 15,000 (top15). Selected precursor ions (highest intense) were isolated in a 1.6 m/*z* window and subjected to fragmentation by higher energy collision induced dissociation using a normalized collision energy of 27 eV. Automatic gain control target values were set to 1×10^6 and 5×10^4 and the maximum ion injection was set to 120 ms and 250 ms for MS and MS/MS, respectively, with 20 s dynamic exclusion. Polysiloxane at *m/z* 371.1012 was used as internal calibrant [40].

Raw data and label free quantification analysis were done with Proteome Discoverer 2.3 (Thermo Fisher Scientific). In the consensus workflow, the Feature Mapper, the Precursor Ion Quantifier and the Protein False Discovery Rate (FDR) Validator nodes were used. With the Feature Mapper node chromatographic runs were aligned based on the retention time. The Precursor Ion Quantifier node parameters for peptides were set to Unique and Razor, precursor abundances were based on intensity, and sample normalization was based on total peptide amount. Target FDR was set to 0.01. For the processing workflow the Minora Feature Detector was used. Raw data were searched against the Uniprot human database (November 2019; 20,609 protein sequences). Mascot and Sequest were applied as search algorithms with the following settings: (1) trypsin as enzyme allowing two missed cleavages, (2) carbamidomethylation of cysteins (+ 57.0214 Da) as fixed modification, (3) oxidation of methionine (+ 15.9949 Da) as variable modification, and (4) mass tolerance for MS and MS/MS were set to 10 ppm and 0.02 Da, respectively. Raw data and Proteome Discoverer search results have been deposited in the ProteomeXchange repository with identifier PXD024106 (username: reviewer_pxd024106@ebi.ac.uk, password: OYobSSEO).

Statistical analysis

Data are expressed as mean ± standard deviation (SD). In case of multiple group comparisons, one-way analysis of variance (ANOVA), two-way ANOVA or two-way repeated measurement ANOVA was used, followed by least significant difference (LSD) tests (one-way ANOVA) or two-tailed *t* tests (two-way ANOVA) as posthoc tests. In

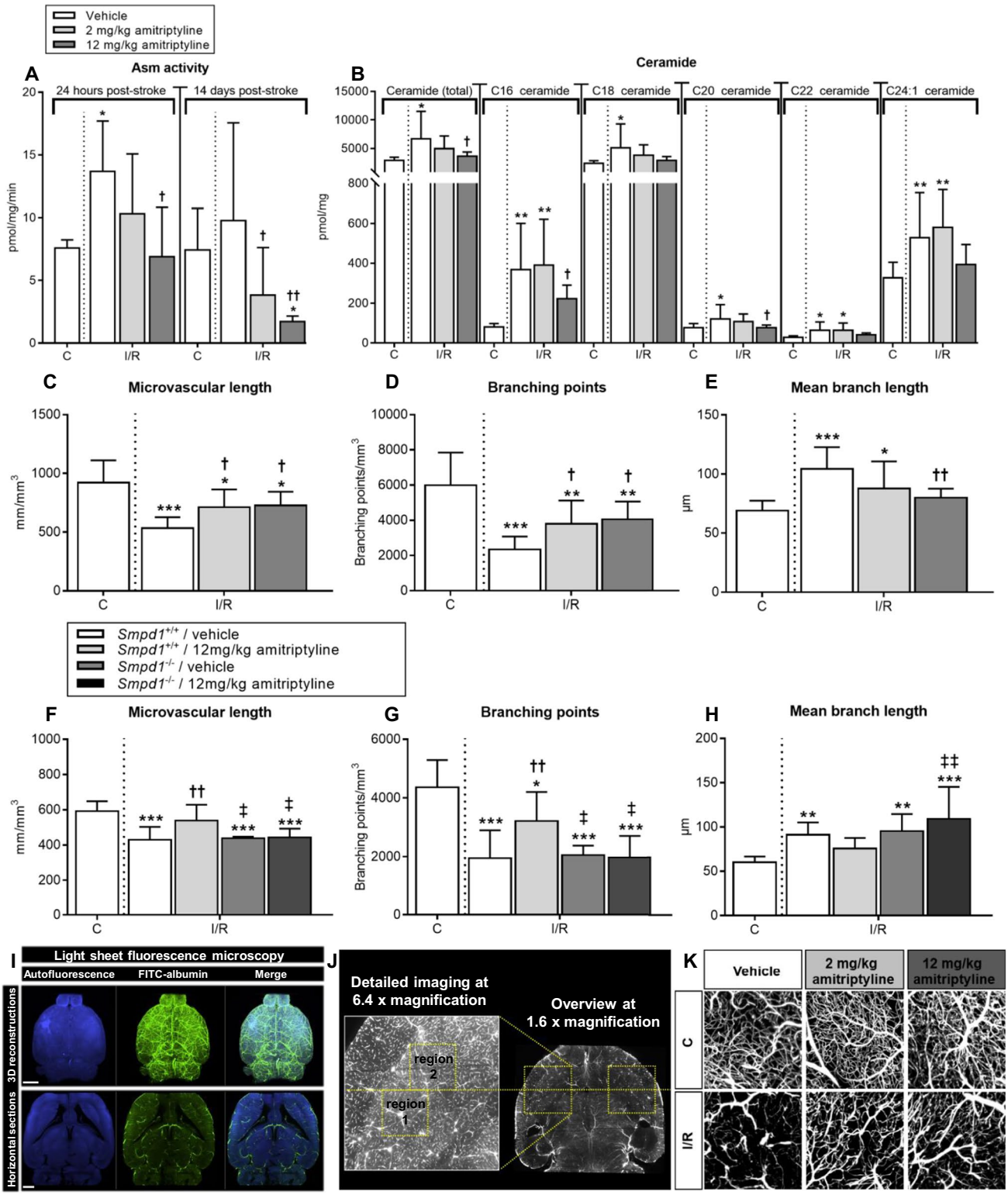

case of comparisons between 2 groups, unpaired or paired two-tailed *t* tests were used. All values were normally distributed. *P* values ≤ 0.05 were defined to indicate statistical significance. The statistical details (*n* numbers, mean ± SD and tests) are given in the figure legends. Sample size planning was conducted with G*Power version 3.1.7 software of the University of Düsseldorf, Germany. Statistical analyses were performed using GraphPad Prism version 7.0 software.

◂**Fig. 1** Amitriptyline inhibits ASM activity in vivo and promotes angiogenesis after I/R in an Asm dependent way. **A** Asm activity in the reperfused ischemic striatum (labeled I/R) and contralateral non-ischemic striatum (labeled C), measured using BODIPY-labeled sphingomyelin in wildtype mice exposed to transient MCAO, which were intraperitoneally treated with vehicle or amitriptyline (2 or 12 mg/kg b.w., b.i.d.) immediately after MCAO or with 24 h delay, followed by animal sacrifice after 24 h or after 14 days. **B** Ceramide content, measured by LC–MS/MS in I/R and C of wildtype MCAO mice treated with vehicle or amitriptyline for 14 days as above. **C** Total microvascular length, **D** branching point density and **E** mean microvascular branch length, evaluated by LSM in I/R and C of wildtype MCAO mice treated with vehicle or amitriptyline for 14 days. **F** Microvascular length, **G** branching point density and (**H**) mean branch length in C and I/R of *Smpd1*$^{+/+}$ (wildtype) and *Smpd1*$^{-/-}$ (that is, ASM-deficient) MCAO mice treated with vehicle or amitriptyline for 14 days. Note that amitriptyline increases angiogenesis in wildtype but not *Smpd1*$^{-/-}$ mice. Representative 3D stacks post-I/R are shown in (**I**), ROIs for the evaluation of microvascular networks in (**J**), and maximum projection images inside these ROIs in (**K**). Data are means ± SD values. *$p \le 0.05$/**$p \le 0.01$/***$p \le 0.001$ compared with non-ischemic C; $^{\dagger}p \le 0.05$/$^{\dagger\dagger}p \le 0.01$ compared with corresponding vehicle; $^{\ddagger}p \le 0.05$/$^{\ddagger\ddagger}p \le 0.01$ compared with corresponding *Smpd1*$^{+/+}$ (n = 4–7 animals/group [in (**A**)]; n = 7–9 animals/group [in (**B**)]; n = 7–8 animals/group [in (**C**–**E**)]; $n = 5$–7 animals/group [in (**F**–**H**)]; analyzed by one-way ANOVA followed by LSD tests). Scale bars in 3D reconstructions in (**I**), 500 µm; in horizontal sections in (**I**), 1000 µm

Data and software ability

G*Power version 3.1.7 software of the University of Düsseldorf, Germany and Image J software are public programs available online without charge. GraphPad Prism version 7.0 software is commercially available via Graphpad Software (San Diego, CA, U.S.A.).

Results

I/R increases brain Asm activity and ceramide level in vivo, which is reversed by the ASM inhibitor amitriptyline

In the reperfused ischemic striatum of vehicle-treated mice we found increased Asm activity at 24 h, but not 14 days post-MCAO (Fig. 1A). Asm inhibition by the tricyclic antidepressant amitriptyline (2 or 12 mg/kg b.i.d.) dose-dependently reduced Asm activity at both timepoints (Fig. 1A). Both long-chain (C16, C18) and very long-chain (C20, C22, C24:1) ceramides were increased predominantly in cerebral microvessels upon I/R, as shown by liquid chromatography tandem–mass spectrometry (LC–MS/MS) combined with immunohistochemistry (Fig. 1B; Suppl. Fig. 1). Amitriptyline reduced ceramide levels (Fig. 1B; Suppl. Fig. 1). This effect similarly affected long-chain and very long-chain ceramides (Fig. 1B). Total sphingomyelin content did not change in response to I/R or amitriptyline (Suppl. Fig. 2). An increase of fusogenic C16 long-chain sphingomyelin and C22 and C24:1 very long-chain sphingomyelin at the expense of the most abundant C18 sphingomyelin was noted following I/R (Suppl. Fig. 2). Sphingosine-1-phospate (S1P), an important mediator of angiogenesis, increased post-I/R, but was not further modulated by amitriptyline (Suppl. Fig. 3A). Amitriptyline applied immediately after I/R reduced infarct volume, but did not alter brain edema or blood–brain barrier permeability assessed by IgG extravasation after 24 h (Suppl. Fig. 4A–C). Conversely, delayed amitriptyline initiated after 24 h did not influence infarct volume after 14 days (3.38 ± 1.22, 3.59 ± 1.17 and 2.89 ± 1.09 mm^3) in mice receiving vehicle, amitriptyline 2 mg/kg b.i.d. and amitriptyline 12 mg/kg b.i.d., respectively). After 24 h, brain infarcts have already maturated, explaining the lack of infarct reduction, when treatment was initiated at this timepoint.

Asm inhibition induces angiogenesis and improves motor-coordination after I/R in vivo

To evaluate consequences of Asm inhibition on neurovascular remodeling, we next examined the architecture of cerebral microvessels by 3D light sheet microscopy (LSM). LSM allows the quantitative analysis of microvascular networks labeled by the microvascular tracer FITC–albumin. Following optical clearing, image segmentation, skeletonization and 3D reconstruction, microvascular network characteristics can be quantified [32, 35]. LSM has strongly advanced the evaluation of cerebral microvessels, which hitherto had been possible ex vivo only to limited extent in 2D sections. Administration of the ASM inhibitor amitriptyline for 14 days or 28 days starting after 24 h increased microvascular density post-I/R, as reflected by an increase in total microvascular length, increase in branching point number and reduction in mean branch length between branching points in the reperfused ischemic striatum (Fig. 1C–E, Suppl. Fig. 5A–C), which is the core of the middle cerebral artery territory. In healthy mice, amitriptyline did not alter the cerebral microvessel characteristics (Suppl. Fig. 6).

Amitriptyline is a functional ASM inhibitor, which also acts as non-selective monoamine reuptake inhibitor and besides has anticholinergic and antihistaminergic properties [26]. To elucidate the role of Asm in amitriptyline's actions, we next examined microvascular network characteristics in *Smpd1*$^{-/-}$ (that is, Asm deficient) mice, which were likewise treated with vehicle or amitriptyline as their wildtype counterparts. Vehicle-treated *Smpd1*$^{-/-}$ mice did not exhibit increased microvascular density post-I/R (Fig. 1F, G). Yet, amitriptyline increased microvascular density in the I/R striatum of *Smpd1*$^{+/+}$ but not *Smpd1*$^{-/-}$ mice, as revealed by an increase in the total microvascular length and the number of branching points (Fig. 1F, G). Mean branch length was not

significantly influenced by amitriptyline in *Smpd1*$^{+/+}$ mice (Fig. 1H). These studies showed that amitriptyline induced the formation of cerebral microvessels via Asm/ceramide pathway inhibition. Representative 3D stacks of transparent brains are shown in Fig. 1I, regions of interest (ROI) used for the evaluation of microvascular network characteristics in Fig. 1J and representative maximum projection images of microvessels inside these ROI of wildtype mice receiving vehicle or amitriptyline in Fig. 1K.

Conventional immunohistochemistry of coronal 2D sections confirmed an increased number of CD31$^+$ microvessels in the I/R striatum of wildtype mice by amitriptyline (Fig. 2A), indicative of enhanced angiogenesis. Asm inhibition reduced IgG extravasation in the brain parenchyma, indicative of intact blood–brain barrier integrity (Fig. 2B), reduced brain infiltrates of CD45$^+$ leukocytes (Fig. 2C) and increased neuronal survival (Fig. 2D) in the I/R striatum. These data provide strong evidence that Asm inhibition entrains a robust brain parenchymal remodeling response. Blood–brain barrier tightening, downscaling of the brain's inflammatory response and promotion of long-term neuronal survival were hallmarks of the successful tissue recovery.

Functional consequences of ASM inhibition post-I/R were evaluated by administration of amitriptyline and the serotonin reuptake inhibitor fluoxetine. Similar to amitriptyline, fluoxetine increased microvascular length and branching point density (Suppl. Fig. 5A, B). Delivery of fluoxetine, but not amitriptyline improved general neurological deficits examined by the Clark score on day 7 post-I/R, enhanced motor-coordination recovery assessed by tight rope tests on day 28 post-I/R and enhanced motor-coordination recovery evaluated by Rotarod tests on days 21 and 28 post-I/R (Suppl. Fig. 5E, G, H). The lack of functional recovery induced by amitriptyline may be attributed to its pleotropic effects on neurotransmitter release, uptake and signaling, in particular to its anticholinergic effects.

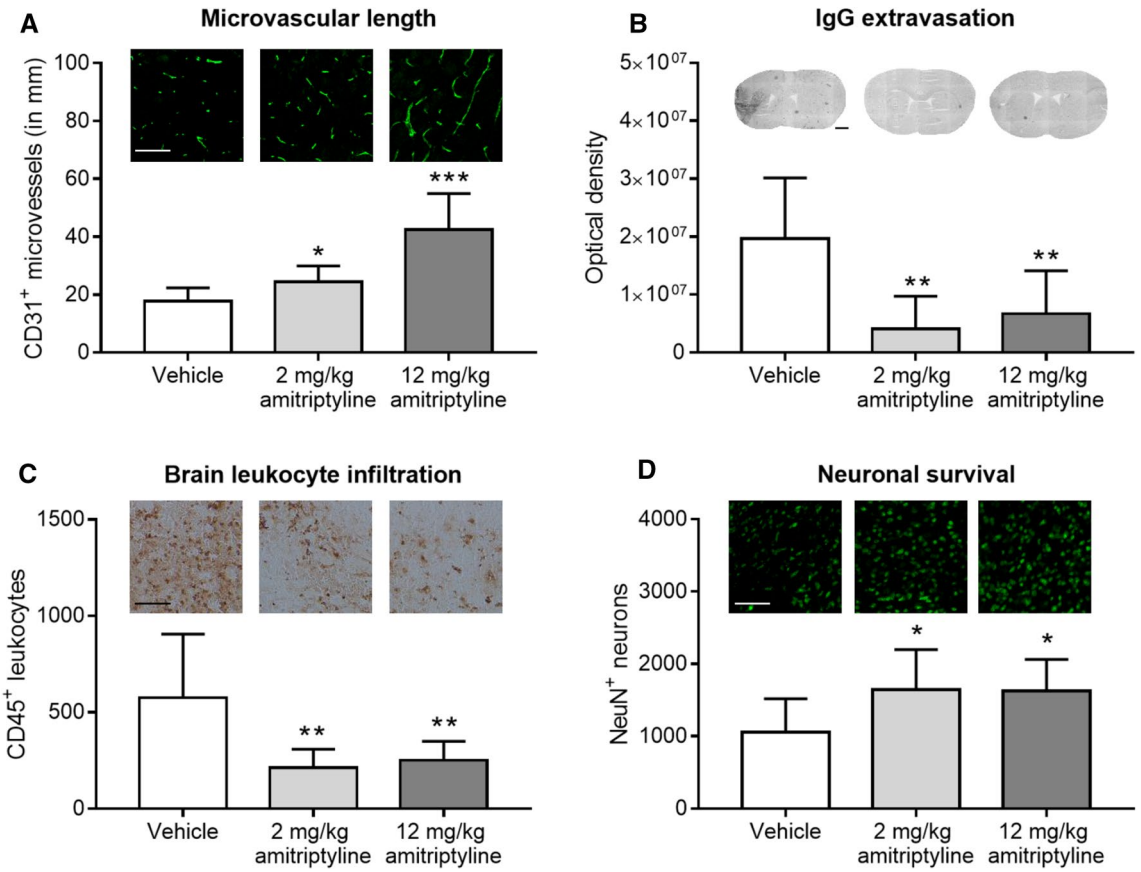

Fig. 2 Asm inhibitor amitriptyline promotes brain remodeling after I/R in vivo when administered with 24 h delay. **A** CD31$^+$ microvessels, **B** serum IgG extravasation into brain parenchyma, **C** infiltrating CD45$^+$ leukocytes and **D** surviving NeuN$^+$ neurons evaluated by immunohistochemistry in the reperfused ischemic striatum of C57BL/6j mice exposed to transient MCAO, which were intraperitoneally treated with vehicle or amitriptyline (2 or 12 mg/kg b.w., b.i.d.) starting 24 h after MCAO, followed by animal sacrifice after 14 days. Representative photographs are also shown. Data are means ± SD values. *$p \le 0.05$/**$p \le 0.01$/***$p \le 0.001$ compared with corresponding vehicle ($n = 6$–8 animals/group; analyzed by one-way ANOVA followed by LSD tests). Scale bars in (**A**, **C**), 100 µm; in (**B**), 1000 µm; in (**D**), 200 µm

Amitriptyline reduces ASM activity of human cerebral microvascular endothelial cells in vitro and decreases the intracellular accumulation of ceramide-rich vesicles that are formed upon I/R

To further examine the effects of ASM inhibitors on cerebral microvessels, we next exposed human cerebral microvascular endothelial cells (hCMEC/D3) to non-ischemic control condition (C), oxygen–glucose deprivation (OGD) as in vitro model of ischemia (I), or OGD followed by reoxygenation/glucose re-supplementation as in vitro model of I/R. In contrast to in vivo conditions, ASM activity decreased after 24 h ischemia (I) or 24 h ischemia followed by 3 or 24 h reoxygenation/glucose re-supplementation (I/R) (Fig. 3A, B). Upon I/R but not I only, ceramide accumulation was found in intracellular vesicles (Fig. 3C, D, Suppl. Fig. 7A). The number of ceramide-rich vesicles reached maximum values at 3 h post-I/R and then returned to baseline levels (Suppl. Fig. 7B). Ceramide-rich vesicles typically had a diameter of ~ 200–250 nm (Suppl. Fig. 7C). Both ASM activity (Fig. 3A, B) and the number of intracellular ceramide-rich vesicles (Fig. 3C, D) were markedly reduced by amitriptyline. RT-qPCR studies revealed that *SMPD1* (i.e., *ASM*) mRNA was abundantly expressed in hCMEC/D3, whereas *SMPD2* (i.e., *NSM1*) and *SMPD3* (i.e., *NSM2*) mRNA levels were low (Suppl. Fig. 8A). A similar distribution, that is, abundant *SMPD1* mRNA but low *SMPD2* and *SMPD3* mRNAs, was detected in primary human brain microvascular endothelial cells (HBMECs) and human umbilical vein endothelial cells (HUVECs) (Suppl. Fig. 8A).

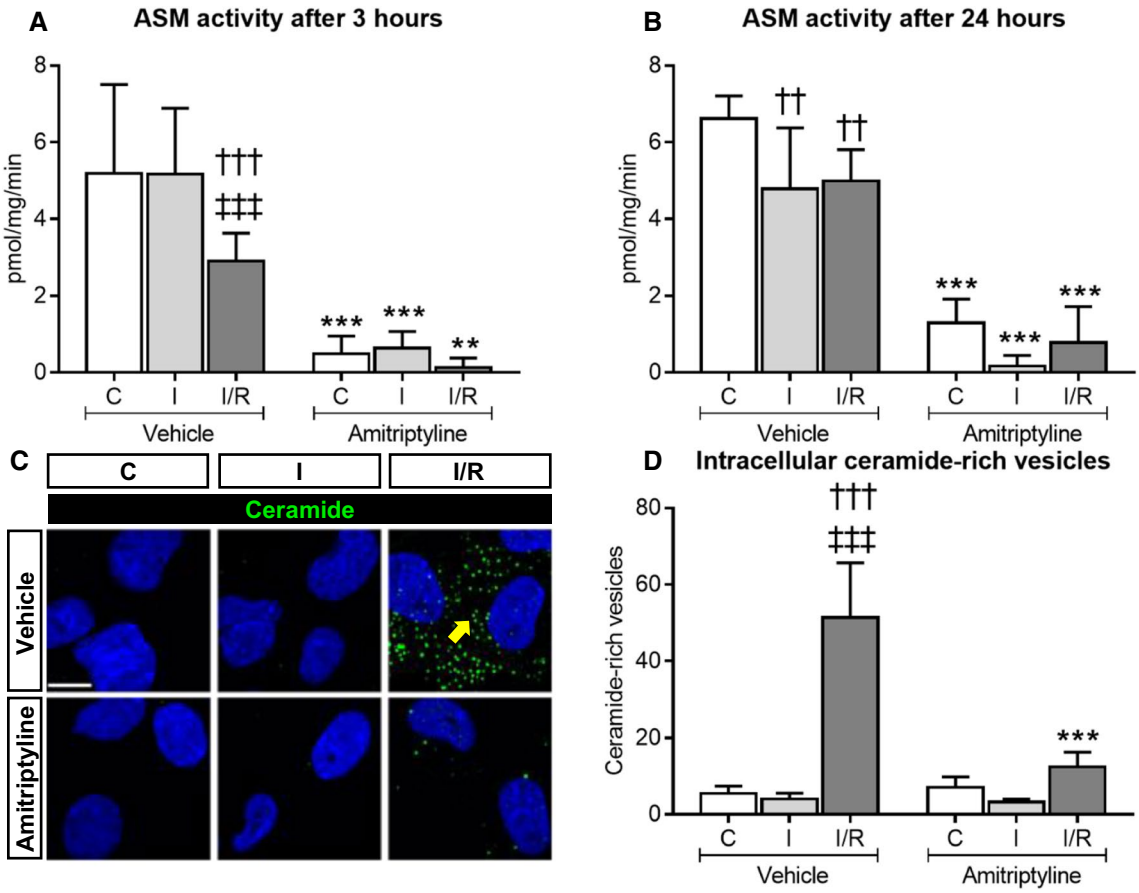

Fig. 3 Amitriptyline inhibits ASM activity in vitro and reduces the intracellular accumulation of ceramide-rich vesicles after I/R. ASM activity, evaluated using BODIPY-labeled sphingomyelin in hCMEC/D3 exposed to **A** non-ischemic control condition (C), 3 h OGD (that is, ischemia; I), or 24 h ischemia followed by 3 h reoxygenation/glucose re-supplementation (I/R), or to **B** non-ischemic C, 24 h ischemia (I) or 24 h ischemia followed by 24 h reoxygenation/glucose re-supplementation (I/R), which were treated with vehicle or amitriptyline (50 µM) during 3 h [in (**A**)] or 24 h [in (**B**)]. Note that ASM activity is reduced by I and I/R. **C** Immunohistochemistry for ceramide in hCMEC/D3 exposed to non-ischemic C, 24 h I or 24 h/3 h I/R treated with vehicle or amitriptyline (50 µM). Note the intracellular accumulation of ceramide-rich vesicles (in green) upon I/R, which is reduced by amitriptyline (selected vesicles labeled with arrow; nuclei were counterstained in blue with Hoechst 33342). The number of vesicles evaluated by Cell Profiler is shown in (**D**). $^{**}p \le 0.01$/$^{***}p \le 0.001$ compared with corresponding vehicle; $^{\dagger\dagger}p \le 0.01$/$^{\dagger\dagger\dagger}p \le 0.001$ compared with corresponding C; $^{\ddagger\ddagger\ddagger}p \le 0.001$ compared with corresponding I ($n = 4$–5 independent samples/group; analyzed by two-way ANOVA followed by LSD tests). Scale bar in (**C**), 10 µm

In these studies, human peripheral blood mononuclear cells (hPBMC), which exhibited high *SMPD3* mRNA levels, served as positive control (Suppl. Fig. 8A). In hCMEC/D3, HBMECs and HUVECs, magnesium dependent NSM (that is, NSM2) activity was by a factor of 45.6 ± 11.7, 58.9 ± 15.3 and 91.4 ± 49.3 lower than whole brain NSM activity (Suppl. Fig. 8B). Delivery of amitriptyline did not influence NSM activity in hCMEC/D3 (Suppl. Fig. 9A, B). In subsequent studies, spiroepoxide and cambinol, but not GW4869 was found to reduce NSM activity in hCMEC/D3 (Suppl. 10A). NSM inhibition by cambinol reduced cell viability but did not decrease sEV release in hCMEC/D3 (Suppl. Fig. 10B–D), as reported for NSM inhibition in other cells [34, 54]. These studies showed that *SMPD1* (ASM) is the predominant sphingomyelinase in endothelial cells.

ASM inhibition by amitriptyline, fluoxetine and desipramine promotes angiogenesis in vitro

Subsequent studies showed that amitriptyline dose-dependently increased the tube formation and transwell migration of hCMEC/D3, increased VEGFR2 abundance on hCMEC/D3 and increased VEGF concentration in the supernatants of hCMEC/D3 (Fig. 4A–H, Suppl. Fig. 18A). At the doses examined, amitriptyline did not influence hCMEC/D3 viability (Suppl. Fig. 11A). Similar findings, that is, elevation of VEGFR2 abundance on endothelial cells and VEGF concentration in supernatants, were made in the murine cerebral endothelial bEND5 cells (Suppl. Fig. 12A, B). Additional studies using the fluoxetine and the tricyclic antidepressant desipramine, which similar to amitriptyline act as ASM inhibitors [27], revealed that fluoxetine and desipramine dose-dependently increased the tube formation and transwell migration of hCMEC/D3 (Fig. 4I–L Suppl. Figs. 18B, C, 19). Again, both inhibitors did not influence hCMEC/D3 viability at the doses administered (Suppl. Fig. 11B, C).

To investigate if the effect of ASM inhibitors on angiogenesis in vitro was related to the inhibition of ASM, we next downregulated *SMPD1* expression by siRNA and examined ASM activity, sphingolipid levels, tube formation, migration and VEGFR2 abundance of hCMEC/D3 in response to amitriptyline. *SMPD1* mRNA level, ASM protein abundance and ASM activity were efficiently reduced by siRNA knockdown by 95.0 ± 1.0%, 86.1 ± 7.4% and 70.1 ± 15.5%, respectively (Suppl. Fig. 13A–C). In response to I/R, *SMPD1* knockdown reduced the number of ceramide-rich intracellular vesicles by 65.6 ± 19.5% (Suppl. Fig. 14A, B). *SMPD1* knockdown did not change the overall ceramide content of hCMEC/D3 assessed by LC–MS/MS (Suppl. Fig. 16A–F), but increased hCMEC/D3 sphingomyelin levels in cells cultured under non-ischemic control conditions (Suppl. Fig. 17A–F). This effect similarly affected long-chain (C16) and very long-chain (C20, C22, C24:1) sphingomyelins. Delivery of *SMPD1* siRNA did not alter S1P levels in hCMEC/D3 (Suppl. Fig. 3B). In vitro, angiogenesis was not influenced by *SMPD1* knockdown (Fig. 4M–P). Yet, amitriptyline increased the tube formation, migration and VEGF secretion of hCMEC/D3 exposed to scrambled (control) siRNA, but not in hCMEC/D3 exposed to *SMPD1* siRNA (Fig. 4M, N, P; Suppl. Figs. 18D, 20A, B), confirming that the induction of angiogenesis was ASM dependent. Treatment of hCMEC/D3 with amitriptyline after *SMPD1* knockdown slightly increased VEGFR2 abundance, which is possibly attributed to remaining residual ASM activity following *SMPD1* siRNA delivery (Suppl. Fig. 13C). hCMEC/D3 viability was not influenced by amitriptyline after *SMPD1* knockdown (Suppl. Fig. 11D).

Ceramide-rich vesicles formed upon I/R are late endosomes/multivesicular bodies (MVBs)

We next explored the nature of the ceramide-rich intracellular vesicles. In histochemical studies, ceramide immunoreactivity did not colocalize with markers of mitochondria (AIF), early endosomes (EEA1), lysosomes (LAMP1), autophagosomes (LC3b) or caveolae (caveolin) (Suppl. Fig. 21). In contrast, partial colocalization was found with markers of late endosomes (Rab7) (Fig. 5A, Suppl. Fig. 22) and MVBs (CD63) (Fig. 5B, Suppl. Fig. 23). MVBs are formed from maturing endosomes by the budding of their limiting membrane into their interior to form intraluminal vesicles called exosomes, which typically have a size of 70–150 nm and which, when released into the extracellular space, have important roles in cell communication [53].

ASM inhibition or *SMPD1* knockdown induces the release of small extracellular vesicles (sEVs) by endothelial cells, which have *bona fide* characteristics of exosomes

Since the number of intracellular ceramide-rich vesicles decreased upon ASM inhibition (see above), we hypothesized that ASM inhibition may have stimulated exosome secretion resulting in the intracellular loss of vesicles. To clarify this hypothesis, we quantified sEVs in the supernatants of hCMEC/D3 exposed to non-ischemic control conditions (C), OGD (labeled I) or OGD followed by reoxygenation/glucose re-supplementation (labeled I/R) which were treated with amitriptyline for 3 or 24 h or exposed to *SMPD1* siRNA knockdown by flow cytometry (Suppl. Fig. 24). I/R increased the number of tetraspanin $CD9^+$ and $CD63^+$ sEVs in supernatants (Fig. 6A–D). This number was further elevated after I/R by amitriptyline (Fig. 6A–D). Likewise, *SMPD1* siRNA knockdown increased the release of $CD9^+$ and $CD63^+$ sEVs by hCMEC/D3 (Suppl. Fig. 14C–F). sEV secretion was

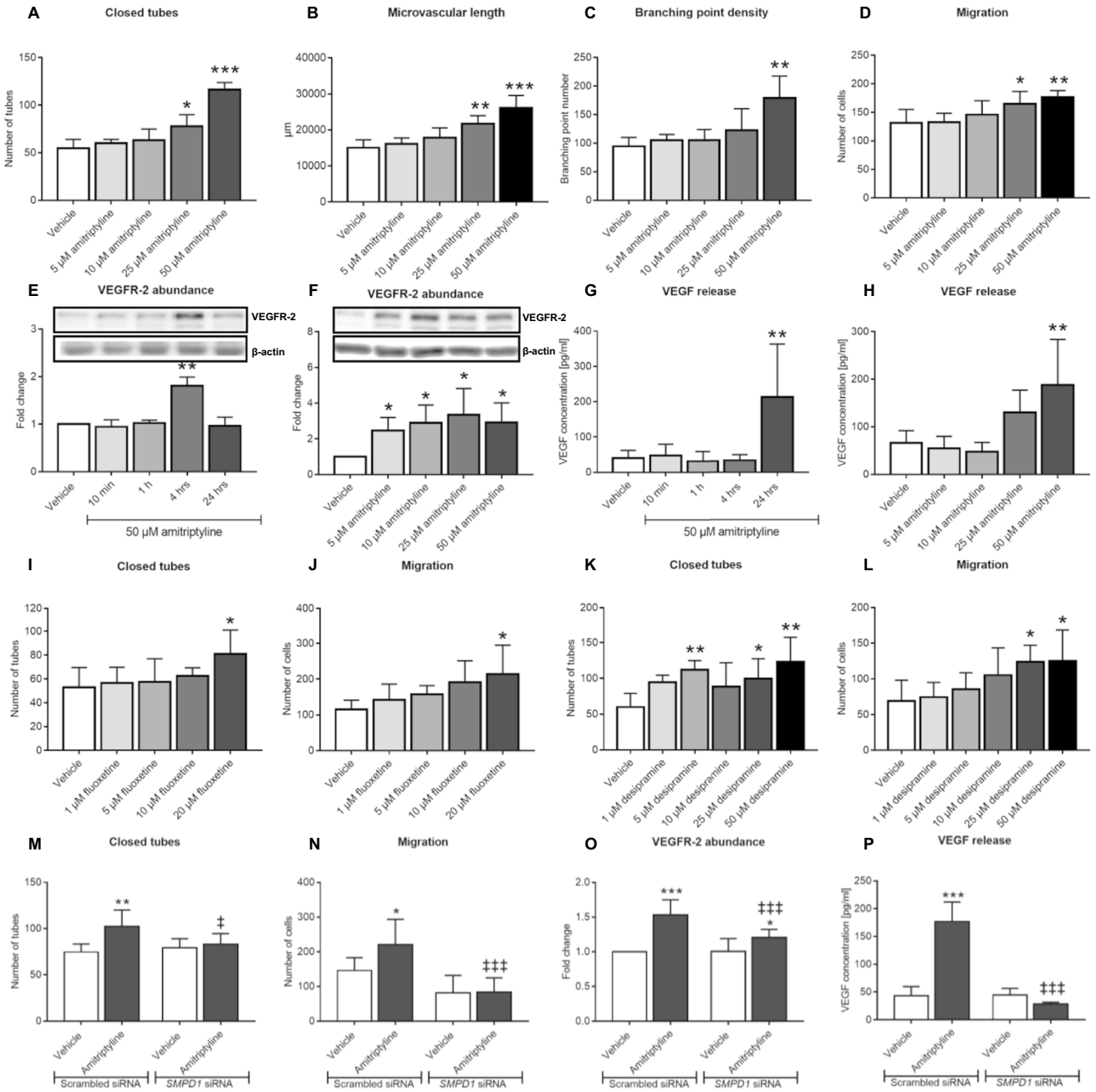

Fig. 4 Amitriptyline, fluoxetine and desipramine promote cerebral angiogenesis in vitro in an ASM dependent way. **A–C** Matrigel-based tube formation evaluated for the number of closed tubes, microvascular length and branching point density, **D** transwell migration, **E**, **F** VEGFR2 abundance examined by Western blot and **G**, **H** VEGF concentration in supernatants measured by enzyme-linked immunosorbent assay (ELISA) of hCMEC/D3 exposed to vehicle or amitriptyline (0–50 µM). In (**F**, **H**), analyses were made after 4 and 24 h amitriptyline exposure, respectively. **I** Tube formation and **J** transwell migration of hCMEC/D3 exposed to vehicle or fluoxetine (0–20 µM). **K** Tube formation and **L** transwell migration of hCMEC/D3 exposed to vehicle or desipramine (0–50 µM). Note that all three ASM inhibitors increase angiogenesis. **M** Tube formation, **N** transwell migration, **O** VEGFR2 abundance and **P** VEGF concentration in supernatants of hCMEC/D3 transfected with scrambled siRNA (used as control) or *SMPD1* siRNA which were exposed to vehicle or amitriptyline (50 µM). In (**O**, **P**), measurements were made after 4 and 24 h amitriptyline exposure, respectively. Data are means ± SD values. $^{*}p \leq 0.05/^{**}p \leq 0.01/^{***}p \leq 0.001$ compared with corresponding vehicle; $^{‡}p \leq 0.05/^{‡‡}p \leq 0.01/^{‡‡‡}p \leq 0.001$ compared with corresponding scrambled siRNA ($n = 3$–7 independent samples/group [in (**A**–**L**)]; n = 5–8 independent samples/group [in (**M,N,O**)]; n = 3 independent samples/group [in (**P**)]; analyzed by one-way ANOVA [in (**A**–**D, G**–**L**)] or two-way ANOVA [in (**M**, **N**, **P**)] followed by LSD tests [in (**A**–**D**, **G**–**N**, **P**)] or paired two-tailed *t* tests [in (**E**, **F**, **O**)])

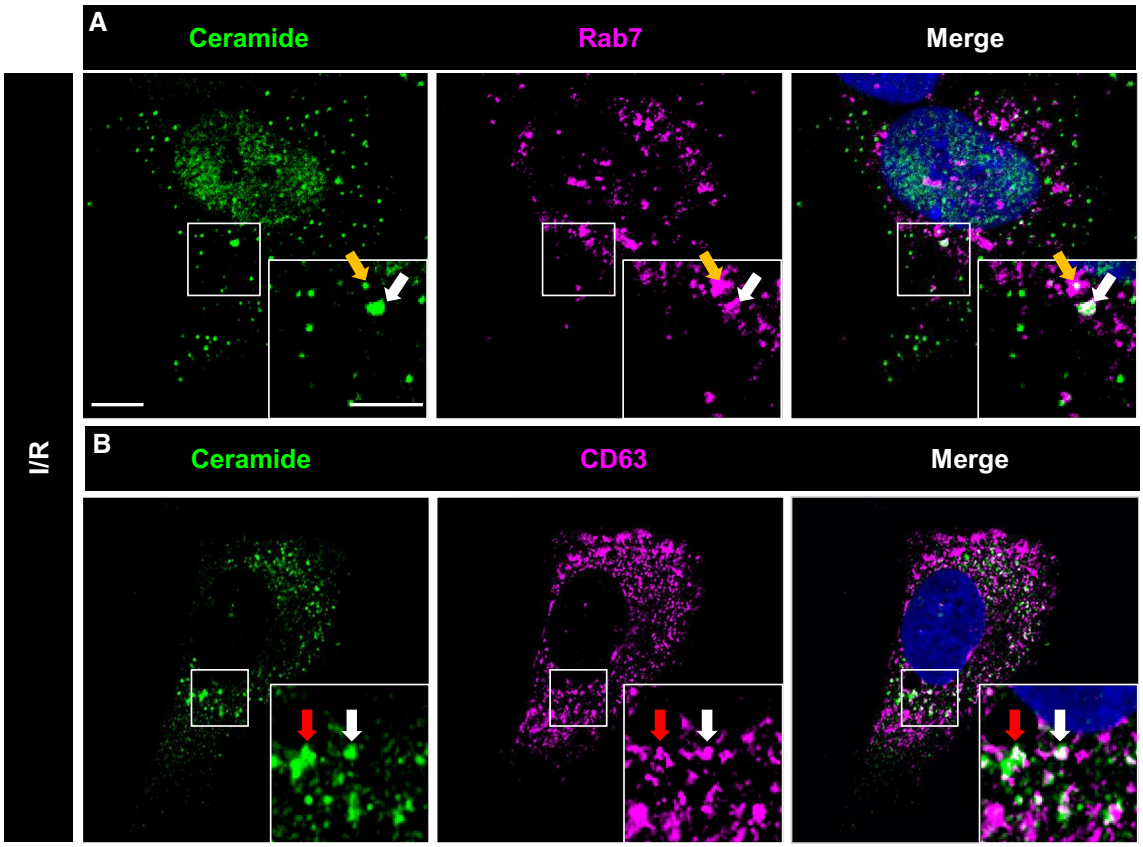

Fig. 5 Intracellular ceramide-rich vesicles express markers of late endosomes and multivesicular bodies. Immunocytochemistry for **A** ceramide (in green) and the late endosome marker Rab7 (in magenta) and **B** ceramide (in green) and the multivesicular body marker CD63 (in magenta) of hCMEC/D3 exposed to 24 h ischemia followed by 3 h reoxygenation/glucose re-supplementation (I/R). In the merged photographs, double labeled cells are shown in white (selected cells labeled with arrow; nuclei were counterstained in blue with Hoechst 33342). Scale bar in overview photograph, 10 µm; in magnification, 5 µm. Data are representative for 3 independent studies

not altered by amitriptyline treatment of hCMEC/D3 subjected to *SMPD1* siRNA knockdown, emphasizing the ASM dependency of vesicle release (Suppl. Fig. 15A–D). Nanoparticle tracking analysis of sEV preparations revealed an average sEV size of 103 ± 35 nm, which is in the range of exosomes (Suppl. Fig. 25A). The particle size distribution of sEVs was not altered by exposure of parental cells to I and I/R or amitriptyline treatment (Suppl. Fig. 25B). Western blots revealed the absence of the cellular contamination marker calnexin and the presence of exosomal markers syntenin and CD9 in sEV preparations (Suppl. Fig. 25C–E). The overall protein content of sEVs was not significantly influenced by functional ASM inhibition (C vehicle: 7.38 ± 3.64 pg/1000 sEVs; C amitriptyline: 8.87 ± 9.04 pg/1000 sEVs; I vehicle 83.01 ± 125.65 pg/1000 sEVs; I amitriptyline 36.06 ± 42.05 pg/1000 sEVs; I/R vehicle 4.61 ± 6.02 pg/1000 sEVs; I/R amitriptyline 23.27 ± 36.59 pg/1000 sEVs). Transmission electron microscopy confirmed that sEVs had the size and cup shape configuration of exosomes (Suppl. Fig. 26).

sEVs released upon ASM inhibitor exposure have angiogenic activity resembling sEVs released upon I/R

Depending on their source and pathophysiological conditions, sEVs have been shown to enhance neurological recovery, brain remodeling and angiogenesis post-I/R [10, 60]. We thus hypothesized that sEVs mediated the angiogenic effects of ASM inhibitors. To test this assumption, we exposed hCMEC/D3 to sEV preparations obtained from supernatants of hCMEC/D3, which had been submitted to non-ischemic control conditions (C), ischemia (I) or ischemia followed by reoxygenation/glucose re-supplementation (I/R) and treatment with vehicle or amitriptyline. As positive control, amitriptyline was administered to hCMEC/D3. Due to limited sEV amounts, the analysis of angiogenic actions of sEVs was confined to in vitro studies. As reported above, amitriptyline increased the tube formation, migration and VEGF secretion of hCMEC/D3 (Fig. 7A–E; Suppl. Fig. 27A, B). sEVs isolated from supernatants of non-ischemic C hCMEC/D3 did not induce hCMEC/D3 tube formation, migration or

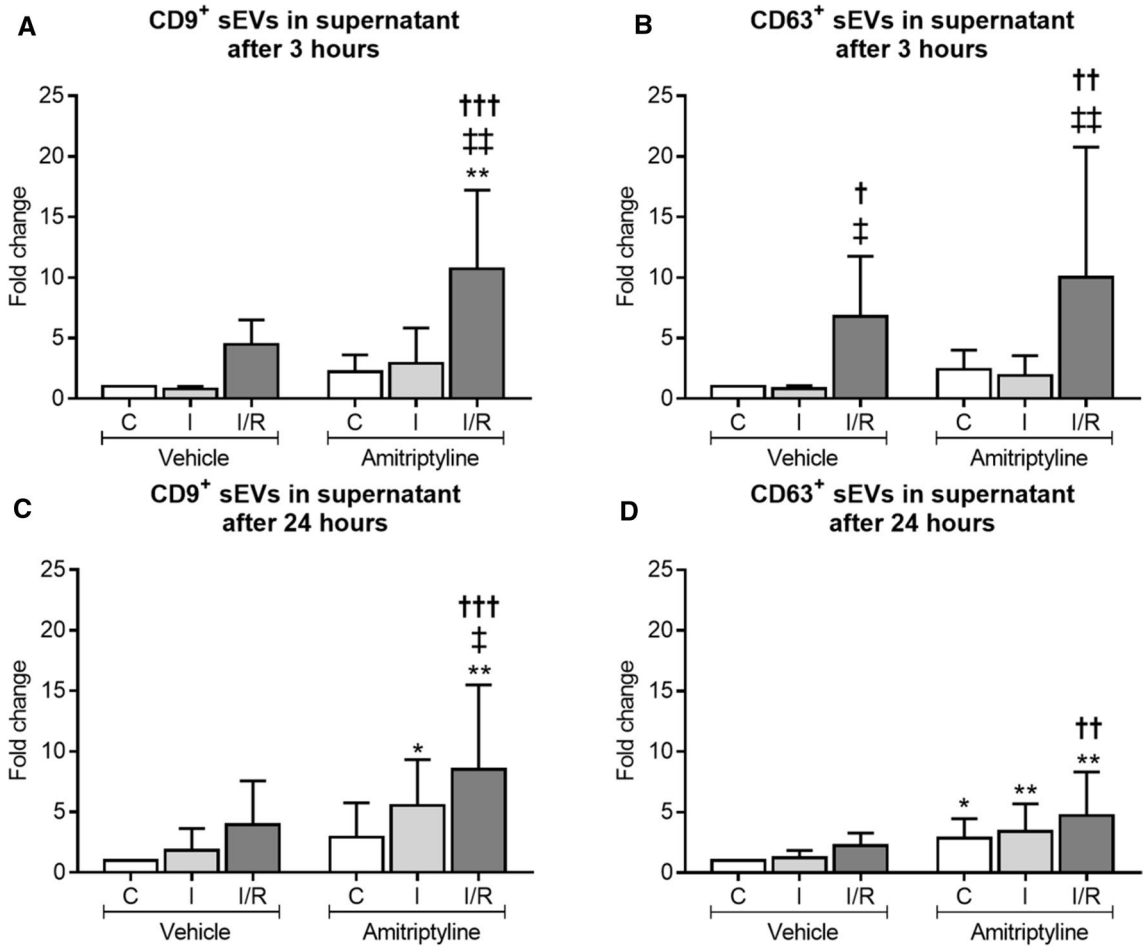

Fig. 6 Amitriptyline promotes the extracellular release of vesicles with immunofluorescence characteristics of exosomes. Concentration of **A**, **C** $CD9^+$ and **B**, **D** $CD63^+$ sEVs in the supernatant of hCMEC/D3 exposed to 3 h C, 3 h I or 24 h/3 h I/R [in (**A**, **B**)] or 24 h C, 24 h I or 24 h/24 h I/R [in (**C**, **D**)] treated with vehicle or amitriptyline (50 µM). sEV concentration was evaluated by AMNIS flow cytometry. Note that the number of $CD9^+$ and $CD63^+$ sEVs, which is elevated upon I/R, further increases by amitriptyline. Data are means ± SD values. $^*p \le 0.05/^{**}p \le 0.01$ compared with corresponding vehicle; $^{\dagger}p \le 0.05/^{\dagger\dagger}p \le 0.01/^{\dagger\dagger\dagger}p \le 0.001$ compared with corresponding C; $^{\ddagger}p \le 0.05/^{\ddagger\ddagger}p \le 0.01$ compared with corresponding I ($n = 4$–5 independent samples/group [in (**A**, **B**)]; $n = 6$–9 independent samples/group [in (**C**, **D**)]; analyzed by two-way ANOVA followed by paired two-tailed *t* tests)

VEGF secretion, whereas sEVs from amitriptyline treated control hCMEC/D3 increased hCMEC/D3 tube formation, migration and VEGF secretion similar to sEVs obtained from hCMEC/D3 exposed to I or I/R (Fig. 7A–E; Suppl. Fig. 27A, B). Since hCMEC/D3 were treated with equal sEV protein amounts, the observed differences in the angiogenic potential of sEVs derived from vehicle-treated non-ischemic hCMEC/D3 compared to sEVs derived from amitriptyline-treated non-ischemic hCMEC/D3 are likely due to differences in the protein cargo. It had previously been shown that sEVs may obtain angiogenic characteristics when their parent cells are exposed to hypoxia [46, 55]. Importantly, amitriptyline did not further elevate the angiogenic activity of sEVs from supernatants of cells exposed to I or I/R (Fig. 7A–E; Suppl. Fig. 27A, B), indicating that amitriptyline mimicked the effect of I or I/R but did not potentiate it.

In contrast to cell samples from hCMEC/D3 treated with 50 µM amitriptyline, in which amitriptyline was detectable by ELISA (0.66 ± 1.32 ng/ml), amitriptyline was not detectable in cell samples from hCMEC/D3 treated with sEVs from amitriptyline (50 µM) treated hCMEC/D3 (0.00 ± 0.00 ng/ml). Hence, the pro-angiogenic effect was not attributed to residual amitriptyline in sEV preparations.

sEVs released upon ASM inhibitor exposure show enhanced uptake by endothelial cells

To elucidate how sEVs released upon ASM inhibitor exposure induce angiogenesis, we next studied sEV uptake by hCMEC/D3. For this purpose, we labeled sEV preparations obtained from vehicle and amitriptyline

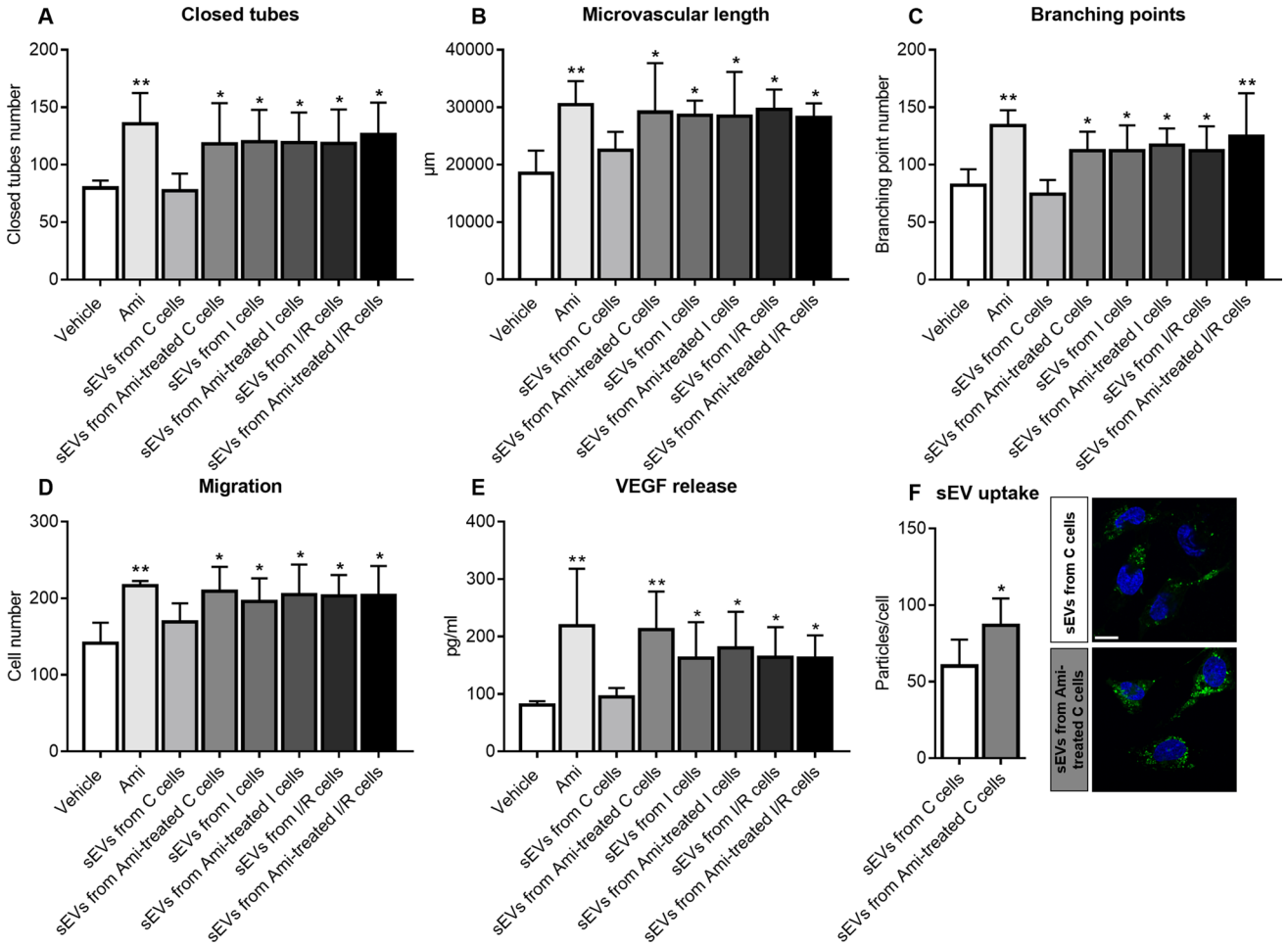

Fig. 7 sEVs released by amitriptyline have angiogenic activity and exhibit enhanced uptake by endothelial cells. **A**–**C** Matrigel-based tube formation, **D** transwell migration and **E** VEGF release of hCMEC/D3, which were treated with vehicle, amitriptyline (Ami, 50 µM) or sEV preparations (25 µg protein/ml) isolated from supernatants of hCMEC/D3 that had been cultured in non-ischemic control condition (C), ischemia (I) or ischemia followed by reoxygenation/glucose re-supplementation (I/R) and had been treated with vehicle or amitriptyline (50 µM) during cell cultivation. VEGF release was determined by ELISA. Representative tube formation and migration assays are shown in Suppl. Fig. 27. **F** hCMEC/D3 uptake of sEV preparations obtained from hCMEC/D3 treated with vehicle or amitriptyline (50 µM) evaluated by PKH67 dye. Representative photographs of hCMEC/D3 exhibiting sEV uptake (in green) are depicted. Nuclei were counterstained in blue with Hoechst 33342. Data are means ± SD values. $*p \leq 0.05$/$**p \leq 0.01$ compared with corresponding vehicle ($n = 4$ independent samples/group [in (**A**–**C**)]; n = 3 independent samples/group [in (**D**)]; $n = 3$–4 independent samples/group [in (**E**)]); $n = 5$ independent samples/group [in (**F**)]; analyzed by one-way ANOVA followed by LSD tests [in (**A**–**E**)], or two-tailed *t* tests [in (**F**)]). Scale bar in (**F**), 10 µm

treated non-ischemic C hCMEC/D3 with a fluorescent dye (PKH67) and then exposed hCMEC/D3 with the labeled preparations. Although sEV preparations obtained from supernatants of endothelial cells exposed to vehicle were reproducibly taken up by hCMEC/D3, this uptake was significantly increased for preparations obtained from supernatants of cells exposed to amitriptyline (Fig. 7F). Immunostaining of recipient hCMEC/D3 revealed the accumulation of labeled particles in $Rab7^+$ late endosomes (Fig. 8A), $CD63^+$ MVBs (Fig. 8B) and $LAMP1^+$ lysosomes (Fig. 8C).

sEVs released by ASM inhibitor carry a protein signature associated with phagocytosis, protein export, extracellular matrix interaction and focal adhesion

By label free proteomics analysis we quantified 1163 proteins with ≤ 2 unique peptides in sEV preparations from supernatants of hCMEC/D3 cultured under normoxia that were treated with vehicle or amitriptyline. Of these, 111 proteins were up-regulated and 9 proteins were down-regulated by at least twofold with a p value ≤ 0.05 in sEVs from amitriptyline treated hCMEC/D3 compared with

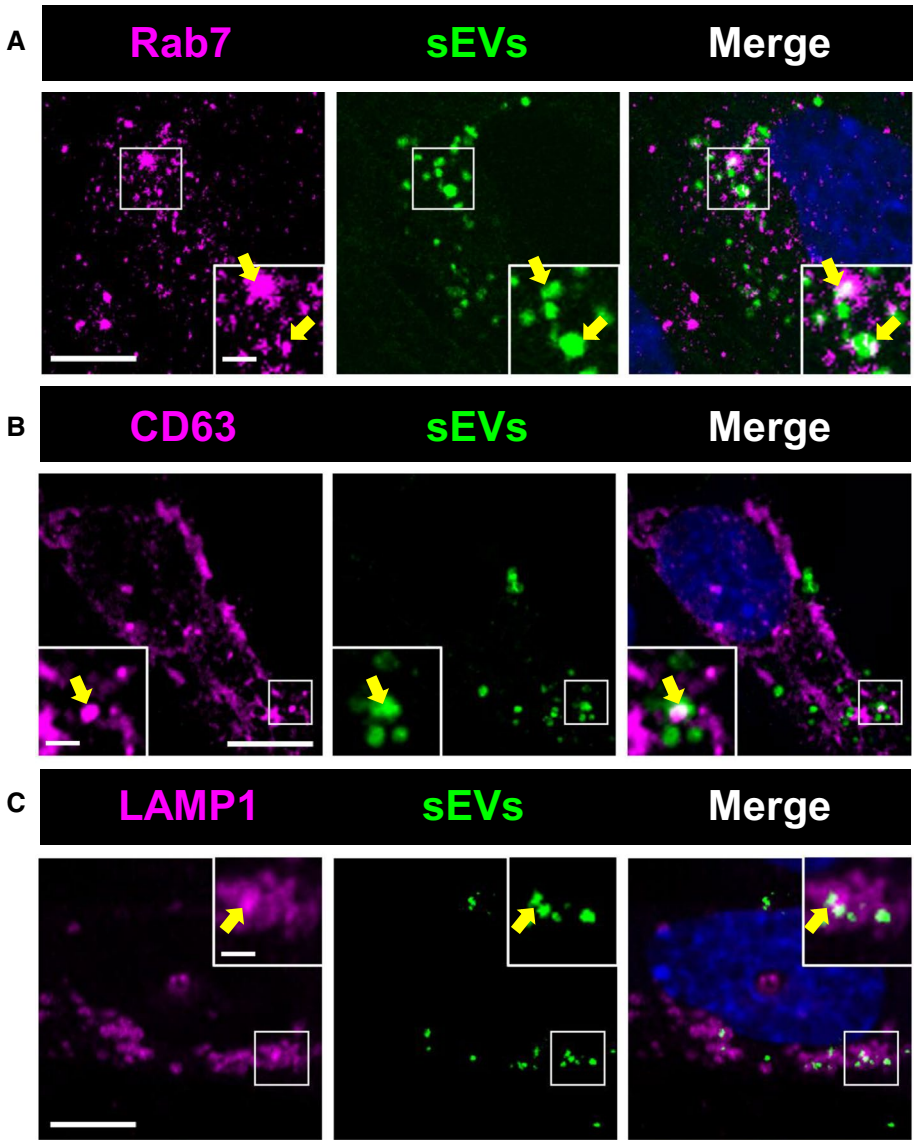

Fig. 8 sEVs taken up by endothelial cells accumulate in late endosomal compartment. hCMEC/D3 exhibiting accumulation of sEV particles labeled with PKH67 (in green) in intracellular vesicles expressing **A** the late endosome marker Rab7, **B** the multivesicular body marker CD63 and **C** the lysosome marker LAMP1 (in magenta). sEV preparations had been obtained from supernatants of hCMEC/D3 treated with amitriptyline (50 µM). Nuclei were counterstained in blue with Hoechst 33342. Scale bar in overview photograph, 10 µm; in magnification, 2 µm. Data are representative of 5 independent studies

sEVs from vehicle treated hCMEC/D3 (Suppl. Fig. 28; Suppl. Tables 1 and 2). KEGG pathway database analysis (https://www.genome.jp/kegg/pathway.html, updated January 2021) showed that up-regulated proteins were implicated in phagosomes (VAMP3, CANX, ITGA5, LAMP1, STX7, HLA-C, HLA-B), protein export (SRP68, SRP72, SRP54) and lysosomes (CTSD, SCARB2, GUSB, GLB1, AP3S1, LAMP1, CTSB, AP1M1) (Suppl. Tables 1 and 3). Downregulated proteins were implicated in extracellular matrix–receptor interactions (TNC, COL4A2) and focal adhesion (TNC, COL4A2) (Suppl. Tables 2 and 3). A list of all quantified proteins containing original data of proteomic measurements is given in Suppl. Table 4.

Discussion

We herein show that the antidepressants amitriptyline, fluoxetine and desipramine, which are diverse regarding their chemical structure and neurotransmitter mode of action, potently promote cerebral angiogenesis in an ASM dependent way when administered in the post-acute stroke phase. Reconstruction of microvascular anatomy using detailed 3D light sheet microscopy analysis [32, 35] allowed us to obtain a comprehensive set of microvascular network characteristics in mice exposed to MCAO that included microvascular density, branching point density

and mean branch length [32, 35]. The in vivo findings were complemented by well-established tube formation, migration and viability assays in vitro using hCMEC/D3 [22, 23]. *Smpd1*$^{-/-}$ abolished angiogenic drug effects in vivo, as did siRNA-mediated *SMPD1* knockdown in vitro. These data proved that ASM inhibition mediated the angiogenic effects of the antidepressants. All three antidepressants, such as several other antidepressants, had been previously shown to act as functional inhibitors of the ASM [27]. In vivo, post-I/R angiogenesis induced by ASM inhibitors was accompanied by enhanced brain parenchymal remodeling, that is, reduced blood–brain barrier permeability, reduced brain leukocyte infiltrates and increased neuronal survival, and in case of fluoxetine with enhanced neurological recovery evaluated by Clark score, tight rope and Rotarod tests. Our study does not provide a direct proof that the enhanced angiogenesis drives brain parenchymal remodeling and neurological recovery. The lack of functional neurological recovery induced by amitriptyline may be attributed to its pleotropic effects on neurotransmitter release, uptake and signaling, in particular its anticholinergic effects. The observation that Asm inhibition promotes angiogenesis post-I/R and enhances post-ischemic brain remodeling is new. In rats, fluoxetine (10 mg/day) reduced infarct volume, brain leukocyte infiltration and neurological deficits, when administered with up to 9 h delay in rats exposed to intraluminal MCAO [29]. In mice, fluoxetine (10 mg/day) or sertraline (20 mg/day) reduced infarct volume when administered with 1 h delay in a photothrombotic stroke model [3, 48]. In addition, in mice, fluoxetine (10 mg/d) increased neurogenesis in the dentate gyrus, when administered with 1 week delay after transient intraluminal MCAO for 4 weeks [28]. Again in mice, nortriptyline (4 mg/kg) reduced infarct volume via mechanisms involving reduced mitochondrial cytochrome C, smac/Diablo and apoptosis-inducing factor release, when administered before transient intraluminal MCAO [62]. To the best of our knowledge, recovery-promoting effects of nortriptyline, amitriptyline or other tricyclic or tetracyclic antidepressants have so far not been studied in the post-acute stroke phase. This is surprising, since antidepressants are frequently prescribed in clinics for the treatment of stroke-associated depression.

Post-I/R, Asm activity and ceramide level are known to be increased in the mouse and rat brain [19, 39, 61]. LC–MS and MS imaging studies in mouse models of permanent or transient MCAO revealed that C18 ceramide, according to our data the most abundant brain ceramide species, was elevated in ischemic brain tissue [1, 37]. One study after transient MCAO in mice found that specifically very long-chain (C22, C24) ceramides were elevated in the ischemic brain[6], whereas another study after photothrombotic stroke in mice also observed elevated long-chain (C16) ceramide [3]. In immunohistochemical studies we now showed elevated ceramide abundance in vivo post-I/R in cerebral microvessels. Both long-chain (C16, C18) and very long-chain (C20, C22, C24:1) ceramides were increased, and amitriptyline reduced the ceramide levels in microvessels. Formation of ceramide in cerebral microvessels and release into the brain parenchyma has previously been observed in the mouse hippocampus in a model of glucocorticosterone-induced depression [15]. In glucocorticosterone-induced depression, amitriptyline prevented the formation and release of ceramide from microvessels [15]. The delivery of neutralizing anti-ceramide antibody reversed the effects of hippocampal extracts on PC12 cell proliferation [15]. Overactivation of Asm has previously been described in cerebral endothelial cells in the aged mouse brain, associated with blood–brain barrier disturbance by increasing caveolae-mediated transcytosis [42]. miR-induced *Smpd1* knockdown and tamoxifen-induced endothelial-specific *Smpd1* knockout reduced blood–brain barrier disturbance, neuronal degeneration in cortex and hippocampus and cognitive impairment in aged mice [42]. It is interesting to note that I/R injury resembles glucocorticosterone-induced depression as well as brain ageing in that all three pathologies exhibit microvascular ASM/ceramide pathway overactivity. It is tempting to speculate to which degree microvascular integrity is compromised in the depressed brain alongside Asm/ceramide overactivation and whether the promotion of microvascular integrity and sprouting contributes to the mood-stabilizing effects of antidepressant drugs in line with enhanced neurogenesis.

In this study, cerebral human microvascular endothelial cells were found to form ceramide-rich late endosomes/MVBs upon I/R, from which sEVs with *bona fide* exosome characteristics were released in response to ASM deactivation, which induced angiogenesis. In oligodendroglial precursor cells, the budding of exosomes from late endosomes was found to be independent of endosomal sorting complex required for transport (ESCRT), but ceramide and NSM2 dependent [34, 54]. The NSM inhibitor GW4869 prevented exosome formation, as did siRNA-mediated NSM2 knockdown [34, 54]. ASM and NSM are localized on the opposite endosomal membrane leaflets, ASM on the luminal leaflet and NSM on the cytosolic leaflet [56]. Concentration gradients of ceramides on the two leaflets are thought to determine membrane curvature, possibly as a consequence of the cone-shaped physicochemical properties of ceramide [54]. A negative curvature is induced on the side of ceramide accumulation which initiates membrane budding towards the opposite side [54]. Further expanding these previous findings we propose that intraluminal membrane budding may be determined by the balance of sphingomyelinase activities on both membrane leaflets and that reduced ASM activity on the luminal leaflet in addition to increased NSM activity might promote intraluminal vesicle budding. According

to our study, NSM2 (*SMPD3*) expression and NSM activity in endothelial cells are low, and NSM deactivation does not influence sEV release in hCMEC/D3. This observation might explain why ASM critically controls exosome release in endothelial cells. Besides ceramides, sphingomyelins critically control membrane fluidity and fusogenicity, increasing exosome release and uptake particularly at low pH [12, 43]. Notably, *SMPD1* knockdown increased hCMEC/D3 sphingomyelin content. The concentration of sphingomyelins in hCMEC/D3 is ~ 20 times higher than that of ceramides. It is, therefore, likely that the sphingomyelin changes contributed to the increased sEV release and uptake, generating a class of sEVs that in view of the inhibition of the proinflammatory ASM/ceramide pathway confers restorative activity. The present study focused on microvascular endothelial responses to ASM inhibitors. It is conceivable that ASM/ceramide deactivation also influences sEV release in other brain cells. However, since physiological ASM expression is significantly higher in brain endothelial cells than in other brain parenchymal cells [21, 42] and since angiogenesis plays a central role in brain parenchymal remodeling, endothelial cells are particularly predisposed as ASM inhibitor targets. By proteome analysis, we identified 111 proteins that were up-regulated and 9 proteins that were down-regulated by amitriptyline in hCMEC/D3 derived sEVs. KEGG pathway analysis showed that up-regulated proteins had roles in phagosomes, protein export and lysosomes, whereas downregulated proteins had roles in extracellular matrix–receptor interactions and focal adhesion. Subsequent studies evaluating the functional role of individual sEV contents are warranted.

Conclusions

ASM inhibition by clinically administered antidepressants induces cerebral angiogenesis in the post-acute stroke phase. Angiogenesis is mediated by sEVs, which as we suggest are released upon alterations of membrane ceramide balance. These sEVs have *bona fide* characteristics of exosomes. Post-I/R, the increased angiogenesis is accompanied by a profound brain remodeling response with increased blood–brain barrier integrity, reduced brain leukocyte infiltrates and increased long-term neuronal survival. The release of sEVs has disclosed an elegant target, via which stroke recovery can be amplified.

Supplementary Information The online version contains supplementary material available at https://doi.org/10.1007/s00395-022-00950-7.

Acknowledgements The authors thank Britta Kaltwasser for technical assistance. Supported by the German Research Foundation (GRK2098 project 259317790 to D.M.H., E.G., R.K. and B.K.; project 389030878 to D.M.H. and M.G.; FOR-2879 project 405358801 to D.M.H., M.G. and C.K.; SFB/TR240 project 374031971 to C.K., SFB-1116 project 236177352 to A.S. and F.A.S.), German Federal Ministry of Education and Science (3DOS, to D.M.H. and B.G.; to A.S. and F.A.S.), North Rhine Westphalian Ministry for Culture and Science (to A.S. and F.A.S.) and E.U. (ERA-NET EuroTransBio-11 project EVTrust [031B0332B] to D.M.H. and B.G.).

Author contributions DMH, EG and RK designed the study. AMY, NH and CB performed the animal experiments. AMY, NH, XZ, MZ and TH conducted the cell culture studies. AMY, NH, XZ, MZ, TH and DMH were responsible for histochemical and molecular biological experiments on tissues and cells, AMY, NH, MG and DMH for light sheet microscopy studies on cleared whole brains. AMY, XZ, TT, VB, MH and BG performed the in-depth characterization of small extracellular vesicles. FS and BK conducted the sphingolipid mass spectrometry studies. FAS and AS provided the proteome mass spectrometry analysis. DMH, AMY and EG drafted the manuscript, all authors revised it.

Funding Open Access funding enabled and organized by Projekt DEAL.

Declarations

Conflict of interest The authors declare that they have no conflict of interest.

Ethics approval Performed with local government approval (North Rhine Westphalian State Agency for Nature, Environment and Consumer Protection, Recklinghausen).

Consent for publication All authors have read and approved the final version of this manuscript.

References

1. Abe T, Niizuma K, Kanoke A, Saigusa D, Saito R, Uruno A, Fujimura M, Yamamoto M, Tominaga T (2018) Metabolomic Analysis of Mouse Brain after a Transient Middle Cerebral Artery Occlusion by Mass Spectrometry Imaging. Neurol Med Chir (Tokyo) 58:384–392. https://doi.org/10.2176/nmc.oa.2018-0054
2. Benjamin EJ, Muntner P, Alonso A, Bittencourt MS, Callaway CW, Carson AP, Chamberlain AM, Chang AR, Cheng S, Das SR, Delling FN, Djousse L, Elkind MSV, Ferguson JF, Fornage M, Jordan LC, Khan SS, Kissela BM, Knutson KL, Kwan TW, Lackland DT, Lewis TT, Lichtman JH, Longenecker CT, Loop MS, Lutsey PL, Martin SS, Matsushita K, Moran AE, Mussolino ME, O'Flaherty M, Pandey A, Perak AM, Rosamond WD, Roth GA, Sampson UKA, Satou GM, Schroeder EB, Shah SH, Spartano NL,

Stokes A, Tirschwell DL, Tsao CW, Turakhia MP, VanWagner LB, Wilkins JT, Wong SS, Virani SS, American Heart Association Council on E, Prevention Statistics C, Stroke Statistics S (2019) Heart Disease and stroke statistics-2019 update: a report from the American Heart Association. Circulation 139:e56–e528. https://doi.org/10.1161/CIR.0000000000000659

3. Brunkhorst R, Friedlaender F, Ferreiros N, Schwalm S, Koch A, Grammatikos G, Toennes S, Foerch C, Pfeilschifter J, Pfeilschifter W (2015) Alterations of the ceramide metabolism in the peri-infarct cortex are independent of the sphingomyelinase pathway and not influenced by the acid sphingomyelinase inhibitor fluoxetine. Neural Plast. https://doi.org/10.1155/2015/503079
4. Burkhart JM, Schumbrutzki C, Wortelkamp S, Sickmann A, Zahedi RP (2012) Systematic and quantitative comparison of digest efficiency and specificity reveals the impact of trypsin quality on MS-based proteomics. J Proteom 75:1454–1462. https://doi.org/10.1016/j.jprot.2011.11.016
5. Chabriat H, Bassetti CL, Marx U, Audoli-Inthavong ML, Sors A, Lambert E, Wattez M, Hermann DM, investigators RBs (2020) Safety and efficacy of GABAA alpha5 antagonist S44819 in patients with ischaemic stroke: a multicentre, double-blind, randomised, placebo-controlled trial. Lancet Neurol 19:226–233. https://doi.org/10.1016/S1474-4422(20)30004-1
6. Chao HC, Lee TH, Chiang CS, Yang SY, Kuo CH, Tang SC (2019) Sphingolipidomics investigation of the temporal dynamics after ischemic brain injury. J Proteome Res 18:3470–3478. https://doi.org/10.1021/acs.jproteome.9b00370
7. Chollet F, Tardy J, Albucher JF, Thalamas C, Berard E, Lamy C, Bejot Y, Deltour S, Jaillard A, Niclot P, Guillon B, Moulin T, Marque P, Pariente J, Arnaud C, Loubinoux I (2011) Fluoxetine for motor recovery after acute ischaemic stroke (FLAME): a randomised placebo-controlled trial. Lancet Neurol 10:123–130. https://doi.org/10.1016/S1474-4422(10)70314-8
8. Clark WM, Lessov NS, Dixon MP, Eckenstein F (1997) Monofilament intraluminal middle cerebral artery occlusion in the mouse. Neurol Res 19:641–648. https://doi.org/10.1080/01616412.1997.11740874
9. Deng X, Yin X, Allan R, Lu DD, Maurer CW, Haimovitz-Friedman A, Fuks Z, Shaham S, Kolesnick R (2008) Ceramide biogenesis is required for radiation-induced apoptosis in the germ line of C. elegans. Science 322:110–115. https://doi.org/10.1126/science.1158111
10. Doeppner TR, Herz J, Gorgens A, Schlechter J, Ludwig AK, Radtke S, de Miroschedji K, Horn PA, Giebel B, Hermann DM (2015) Extracellular vesicles improve post-stroke neuroregeneration and prevent postischemic immunosuppression. Stem Cells Transl Med 4:1131–1143. https://doi.org/10.5966/sctm.2015-0078
11. EFFECTS Trial Collaboration (2020) Safety and efficacy of fluoxetine on functional recovery after acute stroke (EFFECTS): a randomised, double-blind, placebo-controlled trial. Lancet Neurol 19:661–669. https://doi.org/10.1016/S1474-4422(20)30219-2
12. Ermini L, Ausman J, Melland-Smith M, Yeganeh B, Rolfo A, Litvack ML, Todros T, Letarte M, Post M, Caniggia I (2017) A single sphingomyelin species promotes exosomal release of endoglin into the maternal circulation in preeclampsia. Sci Rep 7:12172. https://doi.org/10.1038/s41598-017-12491-4
13. Focus Trial Collaboration (2019) Effects of fluoxetine on functional outcomes after acute stroke (FOCUS): a pragmatic, double-blind, randomised, controlled trial. Lancet (London, England) 393:265–274. https://doi.org/10.1016/S0140-6736(18)32823-X
14. Gorgens A, Bremer M, Ferrer-Tur R, Murke F, Tertel T, Horn PA, Thalmann S, Welsh JA, Probst C, Guerin C, Boulanger CM, Jones JC, Hanenberg H, Erdbrugger U, Lannigan J, Ricklefs FL, El-Andaloussi S, Giebel B (2019) Optimisation of imaging flow cytometry for the analysis of single extracellular vesicles by using fluorescence-tagged vesicles as biological reference material. J Extracell Vesicles 8:1587567. https://doi.org/10.1080/20013078.2019.1587567
15. Gulbins A, Grassme H, Hoehn R, Wilker B, Soddemann M, Kohnen M, Edwards MJ, Kornhuber J, Gulbins E (2016) Regulation of neuronal stem cell proliferation in the hippocampus by endothelial ceramide. Cell Physiol Biochem 39:790–801. https://doi.org/10.1159/000447789
16. Gulbins A, Schumacher F, Becker KA, Wilker B, Soddemann M, Boldrin F, Muller CP, Edwards MJ, Goodman M, Caldwell CC, Kleuser B, Kornhuber J, Szabo I, Gulbins E (2018) Antidepressants act by inducing autophagy controlled by sphingomyelin-ceramide. Mol Psychiatry 23:2324–2346. https://doi.org/10.1038/s41380-018-0090-9
17. Gulbins E, Palmada M, Reichel M, Luth A, Bohmer C, Amato D, Muller CP, Tischbirek CH, Groemer TW, Tabatabai G, Becker KA, Tripal P, Staedtler S, Ackermann TF, van Brederode J, Alzheimer C, Weller M, Lang UE, Kleuser B, Grassme H, Kornhuber J (2013) Acid sphingomyelinase-ceramide system mediates effects of antidepressant drugs. Nat Med 19:934–938. https://doi.org/10.1038/nm.3214
18. Hacke W, Kaste M, Bluhmki E, Brozman M, Davalos A, Guidetti D, Larrue V, Lees KR, Medeghri Z, Machnig T, Schneider D, von Kummer R, Wahlgren N, Toni D, Investigators E (2008) Thrombolysis with alteplase 3 to 4.5 hours after acute ischemic stroke. N Engl J Med 359:1317–1329. https://doi.org/10.1056/NEJMoa0804656
19. Herr I, Martin-Villalba A, Kurz E, Roncaioli P, Schenkel J, Cifone MG, Debatin KM (1999) FK506 prevents stroke-induced generation of ceramide and apoptosis signaling. Brain Res 826:210–219
20. Herz J, Reitmeir R, Hagen SI, Reinboth BS, Guo Z, Zechariah A, ElAli A, Doeppner TR, Bacigaluppi M, Pluchino S, Kilic U, Kilic E, Hermann DM (2012) Intracerebroventricularly delivered VEGF promotes contralesional corticorubral plasticity after focal cerebral ischemia via mechanisms involving anti-inflammatory actions. Neurobiol Dis 45:1077–1085. https://doi.org/10.1016/j.nbd.2011.12.026
21. Jernigan PL, Makley AT, Hoehn RS, Edwards MJ, Pritts TA (2015) The role of sphingolipids in endothelial barrier function. Biol Chem 396:681–691. https://doi.org/10.1515/hsz-2014-0305
22. Jin F, Hagemann N, Brockmeier U, Schafer ST, Zechariah A, Hermann DM (2013) LDL attenuates VEGF-induced angiogenesis via mechanisms involving VEGFR2 internalization and degradation following endosome-trans-Golgi network trafficking. Angiogenesis 16:625–637. https://doi.org/10.1007/s10456-013-9340-2
23. Jin F, Hagemann N, Sun L, Wu J, Doeppner TR, Dai Y, Hermann DM (2018) High-density lipoprotein (HDL) promotes angiogenesis via S1P3-dependent VEGFR2 activation. Angiogenesis 21:381–394. https://doi.org/10.1007/s10456-018-9603-z
24. Jorge RE, Robinson RG, Arndt S, Starkstein S (2003) Mortality and poststroke depression: a placebo-controlled trial of antidepressants. Am J Psychiatry 160:1823–1829. https://doi.org/10.1176/appi.ajp.160.10.1823
25. Kojima T, Hirota Y, Ema M, Takahashi S, Miyoshi I, Okano H, Sawamoto K (2010) Subventricular zone-derived neural progenitor cells migrate along a blood vessel scaffold toward the post-stroke striatum. Stem Cells 28:545–554. https://doi.org/10.1002/stem.306
26. Kornhuber J, Muller CP, Becker KA, Reichel M, Gulbins E (2014) The ceramide system as a novel antidepressant target. Trends Pharmacol Sci 35:293–304. https://doi.org/10.1016/j.tips.2014.04.003
27. Kornhuber J, Tripal P, Reichel M, Terfloth L, Bleich S, Wiltfang J, Gulbins E (2008) Identification of new functional inhibitors of acid sphingomyelinase using a structure-property-activity relation

model. J Med Chem 51:219–237. https://doi.org/10.1021/jm070524a
28. Li WL, Cai HH, Wang B, Chen L, Zhou QG, Luo CX, Liu N, Ding XS, Zhu DY (2009) Chronic fluoxetine treatment improves ischemia-induced spatial cognitive deficits through increasing hippocampal neurogenesis after stroke. J Neurosci Res 87:112–122. https://doi.org/10.1002/jnr.21829
29. Lim CM, Kim SW, Park JY, Kim C, Yoon SH, Lee JK (2009) Fluoxetine affords robust neuroprotection in the postischemic brain via its anti-inflammatory effect. J Neurosci Res 87:1037–1045. https://doi.org/10.1002/jnr.21899
30. Lin DJ, Finklestein SP, Cramer SC (2018) New directions in treatments targeting stroke recovery. Stroke 49:3107–3114. https://doi.org/10.1161/STROKEAHA.118.021359
31. Ludwig KR, Schroll MM, Hummon AB (2018) Comparison of In-solution, FASP, and S-trap based digestion methods for bottom-up proteomic studies. J Proteome Res 17:2480–2490. https://doi.org/10.1021/acs.jproteome.8b00235
32. Lugo-Hernandez E, Squire A, Hagemann N, Brenzel A, Sardari M, Schlechter J, Sanchez-Mendoza EH, Gunzer M, Faissner A, Hermann DM (2017) 3D visualization and quantification of microvessels in the whole ischemic mouse brain using solvent-based clearing and light sheet microscopy. J Cereb Blood Flow Metab 37:3355–3367. https://doi.org/10.1177/0271678X17698970
33. Manoonkitiwongsa PS, Jackson-Friedman C, McMillan PJ, Schultz RL, Lyden PD (2001) Angiogenesis after stroke is correlated with increased numbers of macrophages: the clean-up hypothesis. J Cereb Blood Flow Metab 21:1223–1231. https://doi.org/10.1097/00004647-200110000-00011
34. Menck K, Sonmezer C, Worst TS, Schulz M, Dihazi GH, Streit F, Erdmann G, Kling S, Boutros M, Binder C, Gross JC (2017) Neutral sphingomyelinases control extracellular vesicles budding from the plasma membrane. J Extracell Vesicles 6:1378056. https://doi.org/10.1080/20013078.2017.1378056
35. Merz SF, Korste S, Bornemann L, Michel L, Stock P, Squire A, Soun C, Engel DR, Detzer J, Lorchner H, Hermann DM, Kamler M, Klode J, Hendgen-Cotta UB, Rassaf T, Gunzer M, Totzeck M (2019) Contemporaneous 3D characterization of acute and chronic myocardial I/R injury and response. Nat Commun 10:2312. https://doi.org/10.1038/s41467-019-10338-2
36. Naser E, Kadow S, Schumacher F, Mohamed ZH, Kappe C, Hessler G, Pollmeier B, Kleuser B, Arenz C, Becker KA, Gulbins E, Carpinteiro A (2020) Characterization of the small molecule ARC39, a direct and specific inhibitor of acid sphingomyelinase in vitro. J Lipid Res 61:896–910. https://doi.org/10.1194/jlr.RA120000682
37. Nielsen MM, Lambertsen KL, Clausen BH, Meyer M, Bhandari DR, Larsen ST, Poulsen SS, Spengler B, Janfelt C, Hansen HS (2016) Mass spectrometry imaging of biomarker lipids for phagocytosis and signalling during focal cerebral ischaemia. Sci Rep 6:39571. https://doi.org/10.1038/srep39571
38. Nogueira RG, Jadhav AP, Haussen DC, Bonafe A, Budzik RF, Bhuva P, Yavagal DR, Ribo M, Cognard C, Hanel RA, Sila CA, Hassan AE, Millan M, Levy EI, Mitchell P, Chen M, English JD, Shah QA, Silver FL, Pereira VM, Mehta BP, Baxter BW, Abraham MG, Cardona P, Veznedaroglu E, Hellinger FR, Feng L, Kirmani JF, Lopes DK, Jankowitz BT, Frankel MR, Costalat V, Vora NA, Yoo AJ, Malik AM, Furlan AJ, Rubiera M, Aghaebrahim A, Olivot JM, Tekle WG, Shields R, Graves T, Lewis RJ, Smith WS, Liebeskind DS, Saver JL, Jovin TG, Investigators DT (2018) Thrombectomy 6 to 24 hours after stroke with a mismatch between deficit and infarct. N Engl J Med 378:11–21. https://doi.org/10.1056/NEJMoa1706442
39. Ohtani R, Tomimoto H, Kondo T, Wakita H, Akiguchi I, Shibasaki H, Okazaki T (2004) Upregulation of ceramide and its regulating mechanism in a rat model of chronic cerebral ischemia. Brain Res 1023:31–40. https://doi.org/10.1016/j.brainres.2004.07.024
40. Olsen JV, de Godoy LM, Li G, Macek B, Mortensen P, Pesch R, Makarov A, Lange O, Horning S, Mann M (2005) Parts per million mass accuracy on an Orbitrap mass spectrometer via lock mass injection into a C-trap. Mol Cell Proteom 4:2010–2021. https://doi.org/10.1074/mcp.T500030-MCP200
41. Pariente J, Loubinoux I, Carel C, Albucher JF, Leger A, Manelfe C, Rascol O, Chollet F (2001) Fluoxetine modulates motor performance and cerebral activation of patients recovering from stroke. Ann Neurol 50:718–729
42. Park MH, Lee JY, Park KH, Jung IK, Kim KT, Lee YS, Ryu HH, Jeong Y, Kang M, Schwaninger M, Gulbins E, Reichel M, Kornhuber J, Yamaguchi T, Kim HJ, Kim SH, Schuchman EH, Jin HK, Bae JS (2018) Vascular and neurogenic rejuvenation in aging mice by modulation of ASM. Neuron 100:762. https://doi.org/10.1016/j.neuron.2018.10.038
43. Parolini I, Federici C, Raggi C, Lugini L, Palleschi S, De Milito A, Coscia C, Iessi E, Logozzi M, Molinari A, Colone M, Tatti M, Sargiacomo M, Fais S (2009) Microenvironmental pH is a key factor for exosome traffic in tumor cells. J Biol Chem 284:34211–34222. https://doi.org/10.1074/jbc.M109.041152
44. Reitmeir R, Kilic E, Kilic U, Bacigaluppi M, ElAli A, Salani G, Pluchino S, Gassmann M, Hermann DM (2011) Post-acute delivery of erythropoietin induces stroke recovery by promoting perilesional tissue remodelling and contralesional pyramidal tract plasticity. Brain 134:84–99. https://doi.org/10.1093/brain/awq344
45. Robinson RG, Schultz SK, Castillo C, Kopel T, Kosier JT, Newman RM, Curdue K, Petracca G, Starkstein SE (2000) Nortriptyline versus fluoxetine in the treatment of depression and in short-term recovery after stroke: a placebo-controlled, double-blind study. Am J Psychiatry 157:351–359. https://doi.org/10.1176/appi.ajp.157.3.351
46. Salomon C, Ryan J, Sobrevia L, Kobayashi M, Ashman K, Mitchell M, Rice GE (2013) Exosomal signaling during hypoxia mediates microvascular endothelial cell migration and vasculogenesis. PLoS ONE 8:e68451. https://doi.org/10.1371/journal.pone.0068451
47. Shen Q, Goderie SK, Jin L, Karanth N, Sun Y, Abramova N, Vincent P, Pumiglia K, Temple S (2004) Endothelial cells stimulate self-renewal and expand neurogenesis of neural stem cells. Science 304:1338–1340. https://doi.org/10.1126/science.1095505
48. Shin TK, Kang MS, Lee HY, Seo MS, Kim SG, Kim CD, Lee WS (2009) Fluoxetine and sertraline attenuate postischemic brain injury in mice. Korean J Physiol Pharmacol 13:257–263. https://doi.org/10.4196/kjpp.2009.13.3.257
49. Sokolova V, Ludwig AK, Hornung S, Rotan O, Horn PA, Epple M, Giebel B (2011) Characterisation of exosomes derived from human cells by nanoparticle tracking analysis and scanning electron microscopy. Colloids Surf B Biointerfaces 87:146–150. https://doi.org/10.1016/j.colsurfb.2011.05.013
50. Stinear CM, Lang CE, Zeiler S, Byblow WD (2020) Advances and challenges in stroke rehabilitation. Lancet Neurol 19:348–360. https://doi.org/10.1016/S1474-4422(19)30415-6
51. Sun P, Zhang K, Hassan SH, Zhang X, Tang X, Pu H, Stetler RA, Chen J, Yin KJ (2020) Endothelium-targeted deletion of microRNA-15a/16-1 promotes poststroke angiogenesis and improves long-term neurological recovery. Circ Res 126:1040–1057. https://doi.org/10.1161/CIRCRESAHA.119.315886
52. Thery C, Witwer KW, Aikawa E, Alcaraz MJ, Anderson JD, Andriantsitohaina R, Antoniou A, Arab T, Archer F, Atkin-Smith GK, Ayre DC, Bach JM, Bachurski D, Baharvand H, Balaj L, Baldacchino S, Bauer NN, Baxter AA, Bebawy M, Beckham C, Bedina Zavec A, Benmoussa A, Berardi AC, Bergese P, Bielska E, Blenkiron C, Bobis-Wozowicz S, Boilard E, Boireau W,

Bongiovanni A, Borras FE, Bosch S, Boulanger CM, Breakefield X, Breglio AM, Brennan MA, Brigstock DR, Brisson A, Broekman ML, Bromberg JF, Bryl-Gorecka P, Buch S, Buck AH, Burger D, Busatto S, Buschmann D, Bussolati B, Buzas EI, Byrd JB, Camussi G, Carter DR, Caruso S, Chamley LW, Chang YT, Chen C, Chen S, Cheng L, Chin AR, Clayton A, Clerici SP, Cocks A, Cocucci E, Coffey RJ, Cordeiro-da-Silva A, Couch Y, Coumans FA, Coyle B, Crescitelli R, Criado MF, D'Souza-Schorey C, Das S, Datta Chaudhuri A, de Candia P, De Santana EF, De Wever O, Del Portillo HA, Demaret T, Deville S, Devitt A, Dhondt B, Di Vizio D, Dieterich LC, Dolo V, Dominguez Rubio AP, Dominici M, Dourado MR, Driedonks TA, Duarte FV, Duncan HM, Eichenberger RM, Ekstrom K, El Andaloussi S, Elie-Caille C, Erdbrugger U, Falcon-Perez JM, Fatima F, Fish JE, Flores-Bellver M, Forsonits A, Frelet-Barrand A et al (2018) Minimal information for studies of extracellular vesicles 2018 (MISEV2018): a position statement of the International Society for Extracellular Vesicles and update of the MISEV2014 guidelines. J Extracell Vesicles 7:1535750. https://doi.org/10.1080/20013078.2018.1535750

53. Thery C, Zitvogel L, Amigorena S (2002) Exosomes: composition, biogenesis and function. Nat Rev Immunol 2:569–579. https://doi.org/10.1038/nri855
54. Trajkovic K, Hsu C, Chiantia S, Rajendran L, Wenzel D, Wieland F, Schwille P, Brugger B, Simons M (2008) Ceramide triggers budding of exosome vesicles into multivesicular endosomes. Science 319:1244–1247. https://doi.org/10.1126/science.1153124
55. Umezu T, Tadokoro H, Azuma K, Yoshizawa S, Ohyashiki K, Ohyashiki JH (2014) Exosomal miR-135b shed from hypoxic multiple myeloma cells enhances angiogenesis by targeting factor-inhibiting HIF-1. Blood 124:3748–3757. https://doi.org/10.1182/blood-2014-05-576116
56. Verderio C, Gabrielli M, Giussani P (2018) Role of sphingolipids in the biogenesis and biological activity of extracellular vesicles. J Lipid Res 59:1325–1340. https://doi.org/10.1194/jlr.R083915
57. Verheij M, Bose R, Lin XH, Yao B, Jarvis WD, Grant S, Birrer MJ, Szabo E, Zon LI, Kyriakis JM, Haimovitz-Friedman A, Fuks Z, Kolesnick RN (1996) Requirement for ceramide-initiated SAPK/JNK signalling in stress-induced apoptosis. Nature 380:75–79. https://doi.org/10.1038/380075a0
58. Wang YC, Dzyubenko E, Sanchez-Mendoza EH, Sardari M, Silva de Carvalho T, Doeppner TR, Kaltwasser B, Machado P, Kleinschnitz C, Bassetti CL, Hermann DM (2018) Postacute delivery of GABAA alpha5 antagonist promotes postischemic neurological recovery and peri-infarct brain remodeling. Stroke 49:2495–2503. https://doi.org/10.1161/STROKEAHA.118.021378
59. Ward NS (2017) Restoring brain function after stroke - bridging the gap between animals and humans. Nat Rev Neurol 13:244–255. https://doi.org/10.1038/nrneurol.2017.34
60. Xin H, Li Y, Cui Y, Yang JJ, Zhang ZG, Chopp M (2013) Systemic administration of exosomes released from mesenchymal stromal cells promote functional recovery and neurovascular plasticity after stroke in rats. J Cereb Blood Flow Metab 33:1711–1715. https://doi.org/10.1038/jcbfm.2013.152
61. Yu ZF, Nikolova-Karakashian M, Zhou D, Cheng G, Schuchman EH, Mattson MP (2000) Pivotal role for acidic sphingomyelinase in cerebral ischemia-induced ceramide and cytokine production, and neuronal apoptosis. J Mol Neurosci 15:85–97. https://doi.org/10.1385/JMN:15:2:85
62. Zhang WH, Wang H, Wang X, Narayanan MV, Stavrovskaya IG, Kristal BS, Friedlander RM (2008) Nortriptyline protects mitochondria and reduces cerebral ischemia/hypoxia injury. Stroke 39:455–462. https://doi.org/10.1161/STROKEAHA.107.496810
63. Zhang ZG, Chopp M (2015) Promoting brain remodeling to aid in stroke recovery. Trends Mol Med 21:543–548. https://doi.org/10.1016/j.molmed.2015.07.005